What Causes Tides?

Yongfeng Yang

Bureau of Water Resources of Shandong Province

Corresponding author: Yongfeng Yang (roufeng_yang@outlook.com)

Key Points:

- Tides are spectacular phenomenon on the Earth and presently explained with the equilibrium tide theory and the dynamic tide theory;
- We find the tide-generating force is not appropriate for a watery Earth, this makes the presently theories of tides become groundless;
- Alternatively, we propose the elongated spinning of solid Earth shakes ocean basin, thereby forming regular movement of water between all parts of the basin.

Abstract Tides represent the daily regular alternation of high and low waters at the coasts and in the oceans. This movement of water is usually explained with two paradigms: one is the equilibrium tide theory in which the tide-generating force yields a pair of water bulges, and another is the dynamic tide theory in which the tide-generating force makes water move like wave. In this study, we investigate to find that the tide-generating force is derived from a solid Earth, but its application to a fluid (watery) Earth is not too realistic, this makes the two paradigms become groundless. We here propose, the tide-generating force elongates the solid Earth, the spinning Earth allows the solid bulges to shake ocean basins, thus forming daily regular movement of water between all parts of the basins as well as the rise and fall of water levels around the globe. A tide prediction model is developed to show that the predicted tides are morphologically consistent with the observed tides, the average *RMS* calculated against observations for 110 globally tide-gauge stations are 15.17 cm; A further tide prediction comparison shows that the tide made by this model performs slightly better than that made by harmonic analysis, among the selected 56 sample stations, the *RMS* calculated against observations for 31 stations in this model is less than the *RMS* calculated in harmonic analysis.

Plain Language Summary

Tides are extremely spectacular phenomenon on the Earth, explaining them has undoubtedly tested many people including Aristotle, Galileo, Newton, Descartes, and Laplace. The presently explanation of tides are made through the equilibrium tide theory and the dynamic tide theory, both of them are on basis of the tide-generating force. In this work we investigate to find that the tide-generating force is derived from the solid Earth, but its application to a watery Earth is not too realistic because of the property of water, this makes the presently theories of tides become groundless. We here propose, the tide-generating force results in a pair of solid bulges on the Earth, the daily elongating spinning of the solid Earth shakes ocean basins, thereby forming regular water movements around the globe. This newly proposed theory challenges the conventional thinking of tides.

1 Introduction

From antiquity, the regular rising and falling movements of water in the coastal seas have been recognized. Since these movements of water are closely related to frequent coastal activities, explaining them has undoubtedly tested human wisdom. Aristotle (384-322 BC) was highly perplexed by tides, and he vaguely attributed them to the rocky nature of the coastline. The early Chinese considered tides to be the beating of the Earth's pulse or caused by the breathing of the Earth. Others believed tides to be caused by the different depths of ocean water. Galileo theorized that the rotation of the Earth around the Sun and its axis induced motion within the sea to generate the tides. The majority certainly linked tidal action to the influence of the Moon and Sun. Seleucus (2nd century BC) was the first to consider this connection and concluded that the height of the tide was correlated with the Moon's position relative to the Sun. However, determining how the Moon and Sun caused the tides was unknown. A few Arabic explanations proposed that the Moon used its rays to heat and expand the water. Descartes argued that the resulting stresses between the ether and the Earth's surface gave birth to tides when the Moon orbited the Earth. Kepler defined tidal action as the attraction of the Moon and Sun to Earth's water. A more exact solution to this issue was realized by Newton that the Moon's gravitational attraction raises sea water forming the tides, this explanation was further developed into the equilibrium tide theory in which the tide-generating force yields a pair of water bulges. As the equilibrium tide theory does not consider the influences of these factors such as landmass, water depth, the Coriolis force, and friction, the double water bulge is thought to be unrealistic. Together with the subsequent endeavors of Pierre-Simon Laplace, William Thomson, Baron Kelvin, Henri Poincaré, and Arthur Thomas Doodson, the tides were explained with the dynamic tide theory in which the tide-generating force makes water move like wave (Pugh, 1987; Cartwright, 1999; Deacon, 1971; Pugh and Woodworth, 2014; Gerkema, 2019). During the past five decades, our understanding of tides has greatly improved. The rapid development of ocean tide models has facilitated spatial and ground measurements of tides (Pekeris and Accad, 1969; Schwiderski, 1979; Shum et al., 1997; Fu and Cazenave, 2001; Visser et al., 2010; Stammer et al., 2014; Hart-Davis et al., 2021), both tidal dynamics and energy dissipation have also been studied (Stammer et al., 2014), and internal tides investigations are considerably active (Gargett and Hughes, 1972; Phillips, 1974; Shepard, 1975; Garrett and Munk, 1979; Gao et al., 2013; Shanmugam, 2014; Gerkema, 2019). However, although the two explanations of tides coexist

usually, there remains a point that the application of the tide-generating force to a fluid (watery) Earth might not be realistic because of the property of water. Some people believe that more than 70% of the Earth's surface is covered with deep oceans, under the tide-generating force the ocean water would trend to follow towards the Earth-Moon line, it is likely to form a pair of water bulges. In addition, although the tidal waves are thought to be a consequence of the complex ocean response to the gravitational forcing, but how they are initiated by the tide-generating force remains poorly understood, this makes the dynamic tide theory become elusive. Clarifying these issues is particularly important because they are related to the foundation of modern tidal theory. In this work, we investigate this issue with the hope of expanding our understanding of tides.

2 Examination of the existing explanations of tides

2.1 How do these explanations work?

The existing understanding of tides begin with a derivation of the tide-generating force. It is firstly assumed that the Earth orbits about the common center of mass of the Earth-Moon system; this rotation makes all of Earth's particles travel around in circles of the same radius (Figure 1(A)). An identical orbit allows these particles to gain an identical centrifugal force. For particles closer to the Moon, the Moon's gravitational force is greater than the centrifugal force, whereas for particles farther away from the Moon, the Moon's gravitational force is weaker than the centrifugal force. The difference between the centrifugal force and the Moon's gravitational force yields a tide-generating force. This force is further decomposed into a tangential component and a vertical component, the tangential component is along the Earth's surface and called the tractive force (Figure 1(B)). It is necessary to note that a mathematical expression of the tractive force is generally made through the potential field. From this point, two paradigms are conceived for the tides.

One is to use the tractive force to pull the water to flow, with the assumptions that a layer water of same depth covers the Earth, and there are no landmass, the Coriolis force, and friction, and that the water's response to the tidal forcing is immediate, the upshot is that a pair of water bulges is formed along the direction of the Earth-Moon line and a water depression is formed in a ring around the Earth halfway between the two bulges of water (Pugh, 1987; Pugh and Woodworth, 2014). As the Earth spins, an Earthly site would pass these bulges and depression of

water and hence undergo regular alternation of high and low waters per day. Similarly, the Earth orbits about the Sun, and the resulting tractive force yields another pair of water bulges and another water depression. When these two types of water bulges and water depression are combined, they reinforce or cancel each other to yield two fortnightly cycles of the alternation of high and low waters per month. This paradigm is called the equilibrium tide theory and popular in both print and online forms. A more detailed description of the equilibrium tide theory may be found in the cited works (Pugh, 1987; Pugh and Woodworth, 2014; Robert, 2008).

Another is to use the tractive force to drive the water, in consideration of the existences of water depth difference, landmass, the Coriolis force, and friction, with the assumption that the water's response to the tidal forcing is slow, the upshot is that the water moves like wave. Since the resulting tidal wave holds the same frequency as the tide-generating force does, this corresponds to the regular alternation of high and low waters per day. When the lunar tidal forcing and the solar tidal forcing are combined, they reinforce or cancel each other to yield two cycles of the alternation of high and low waters per month. To describe the water movement around a rotating Earth, the hydrodynamic equations of continuity and momentum and the theoretical ideas of wave (i.e., progressive and standing wave, resonance, Kelvin wave, amphidrome system) are nicely developed. This paradigm is called the dynamic tide theory and currently adopted by the tide researchers. A more detailed description of the dynamic tide theory may refer to these works (Schureman, 1940; Doodson and Warburg, 1941; Pugh, 1987; Cartwright, 1999; Deacon, 1971; Pugh and Woodworth, 2014; Gerkema, 2019).

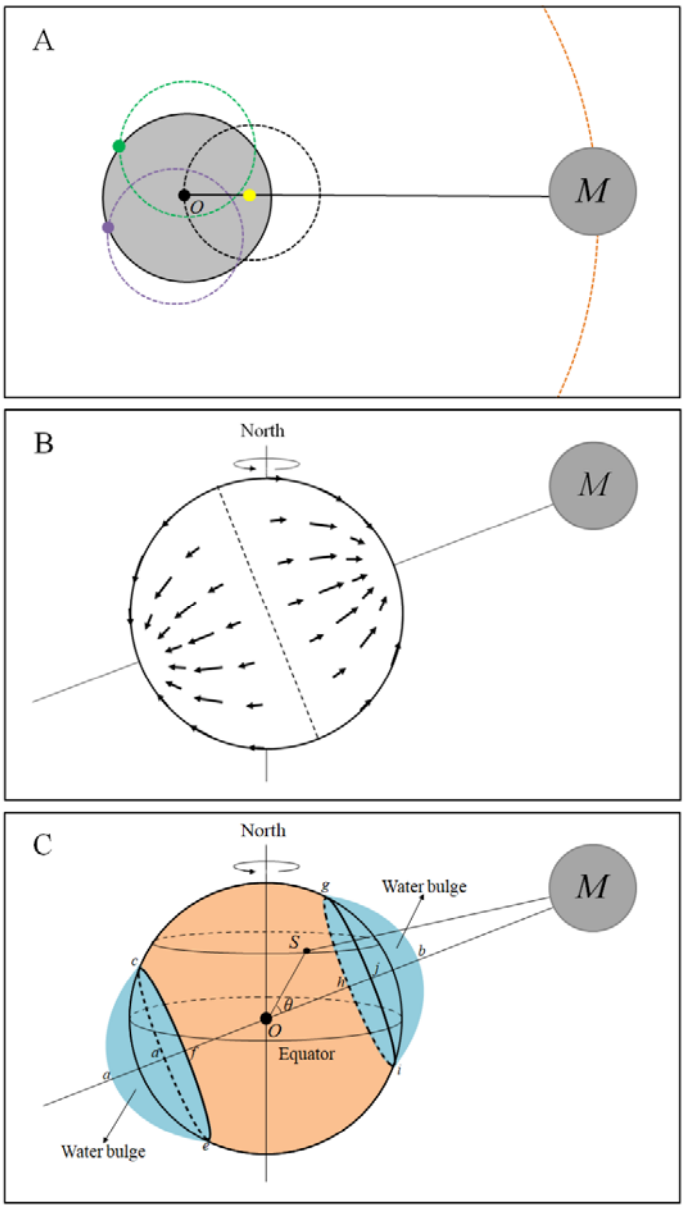

Figure 1. (A) Modeling the movements of the particles in the Earth's body when the Earth rotates about the common center of mass of the Earth-Moon system, which is indicated by a yellow dot. *E* and *M* denote the Earth and the Moon, respectively. Black, green, and purple dots denote one particle in the Earth's center and two particles on the Earth's surface. Black, green, purple, and orange dashed circles denote the orbital movements of these particles and the Moon. (**B**) **Modeling the distribution of the tractive force around the Earth's surface. (C) Model of the two water bulges.** *O* and *M* denote the Earth's center and the Moon, respectively.

θ is the lunar angle of an Earthly site (marked with *S*). Note that the two water bulges are highly exaggerated in this figure.

2.2 What is the trouble with these explanations?

The derivation of the tide-generating force is based on the assumption that all of the particles in the Earth's body execute an identical orbit as the Earth orbits about the common center of mass of the Earth-Moon system, this yields an identical centrifugal force for all of the particles. A combination of this centrifugal force and the Moon's gravitational force results in the tide-generating force. Subsequently, this force (i.e., the horizontal tractive force) is applied to a fluid (watery) Earth. Practically, the particles within a water body are extremely difficult to follow an identical orbit when the water body moves along a curved path, this is because water particles are weakly connected to each other and the low viscosity of water allows water particles to flow freely, the water body's shape can be easily deformed by external force. Refer to Figure 1(A), living practice would show that a watery sphere (marked with gray) is very difficult to remain its shape when it moves along a curved path. In contrast, the particles within a solid body are fixed together, this binding allow solid particles to easily follow an identical orbit when the solid body moves along a curved path. This demonstration leads to a point that the derivation of the tide-generating force is appropriate for a solid Earth rather than for a fluid (watery) Earth, consequently, the equilibrium tide theory and the dynamic tide theory become groundless. Further, the double water bulge and the tidal wave cannot be realized by the tide-generating force. Below, evidence is provided for this expectation.

The two bulges of water are directed along the Earth-Moon line and the water depression is directed orthogonal to the Earth-Moon line. This frame of the two bulges and water depression is outlined in Figure 1(C). Areas *a-cdef* and *b-ghij* represent the two bulging water regions, while area *cdef-ghij* represents the water depression. It may be expected, if there were the two bulges of water and the water depression on the Earth's surface, then an Earthly site (marked with *S*, for instance) would pass these bulges demonstrating high water behavior and pass the depression demonstrating low water behavior as the Earth spins around its axis.

Geometrically speaking, if an Earthly site's lunar angle (i.e., the angle of a site and the Moon relative to the Earth's center) falls into a phase of 0°~45° or 135°~180°, it represents this site enters into one of the two water bulges, and if the lunar angle falls into a phase of 45°~135°, it

represents this site enters into the water depression. Then, the water level variation of a site and its lunar angle can be correlated together. This treatment may be twofold: to verify the existence of a pair of water bulges and the water depression, and to find evidence for new insights. To examine this expectation, two sets of data are employed.

The first is hourly tide-gauge data covering the period from 2014/08/01 to 2014/08/30 from 169 sites belonging to a belt between 45°N and 45°S are selected from the GLOSS database, UHSLC (Caldwell et al., 2015). As the Moon's position transfers between north and south, and its declination varies dominantly between 18°N and 18°S, such a belt allows these sites to smoothly pass the two bulges and depression of water. In the GLOSS database, 189 UHSLC sites are geographically located in the belt, but 20 sites hold incomplete data during this period. A geographic distribution of these 169 sites is listed in Table 1. It is important to note that there are meteorological variations that influence the observed water levels, but GLOSS database do not show information whether these variations are removed or not. From the standpoints of the author, the present status of this work may allow to neglect this influence. A statistical description of the number of high and low water events for these sites is shown in Figure 2. The high water events occur dominantly in the 45°-135° phases, while the low water events occur dominantly in the 0°-45° and 135°-180° phases. From 2014/08/01 to 2014/08/30, these sites yield a total of 121680 hourly data points. Of these data points, approximately 43.42% of the points that fall into the 0°-45° and 135°-180° phases show high water behavior, whereas approximately 46.46% of the points that fall into the 45°-135° phase show low water behavior. These results tend to support that the two bulges and depression of water do not exist.

Table 1(A) Location information of 169 tide-gauge stations from GLOSS database

ID	Name	Latitude (°)	Longitude (°)	ID	Name	Latitude (°)	Longitude (°)
1	POHNPEI	6.98	158.2	223	DAKAR	14.67	342.57
2	BETIO	1.37	172.93	235	PALMEIRA	16.75	337.02
3	BALTRA	0.43	269.72	242	KEY	24.55	278.18
5	MAJURO	7.1	171.37	245	SAN	18.47	293.88
7	MALAKAL	7.33	134.47	253	NEWPORT	41.5	288.67
8	YAP	9.52	138.13	257	SETTLEMENT	26.72	281
9	HONIARA	-9.43	159.95	259	BERMUDA	32.37	295.3
11	CHRISTMAS	1.98	202.53	260	DUCK	36.18	284.27
14	FRENCH	23.87	193.72	261	CHARLESTON	32.78	280.07
15	PAPEETE	-17.53	210.43	264	ATLANTIC	39.35	285.58
16	RIKITEA	-23.13	225.05	268	LIMON	10	276.97
18	SUVA	-18.13	178.43	271	FORT	14.6	298.93
19	NOUMEA	-22.3	166.43	283	FORTALEZA	-3.72	321.53
21	JUAN	-33.62	281.17	289	GIBRALTAR	36.12	354.65
22	EASTER	-27.15	250.55	291	ASCENSION	-7.92	345.58
23	RAROTONGA	-21.2	200.22	302	BALBOA	8.97	280.43
24	PENRHYN	-8.98	201.95	328	KO	11.8	99.82
25	FUNAFUTI	-8.53	179.22	329	QUARRY	22.3	114.22
29	KAPINGAMARANGI	1.1	154.78	331	BRISBANE	-27.37	153.17
30	SANTA	0.75	269.68	332	BUNDABERG	-24.83	152.35
31	NUKU	-8.93	219.92	333	FORT	-33.85	151.23
34	CABO	22.88	250.08	334	TOWNSVILLE	-19.25	146.83
38	NUKU'ALOFA	-21.13	184.83	335	SPRING	-42.55	147.93
43	PALMYRA	5.87	197.9	336	BOOBY	-10.6	141.92
46	PORT	-17.77	168.3	340	KAOHSIUNG	22.62	120.28
47	CHICHIJIMA	27.1	142.18	341	KEELUNNG	25.15	121.75
49	MINAMITORISHIMA	24.3	153.97	347	ABASHIRI	44.02	144.28
50	MIDWAY	28.22	182.63	348	HAMADA	34.9	132.07

51	WAKE	19.28	166.62	349	TOYAMA	36.77	137.22
52	JOHNSTON	16.75	190.48	350	KUSHIRO	42.97	144.38
53	GUAM	13.43	144.65	351	OFUNATO	39.07	141.72
55	KWAJALEIN	8.73	167.73	352	MERA	34.92	139.83
56	PAGO	-14.28	189.32	353	KUSHIMOTO	33.47	135.78
57	HONOLULU	21.3	202.13	354	ABURATSU	31.57	131.42
58	NAWILIWILI	21.97	200.65	355	NAHA	26.22	127.67
59	KAHULUI	20.9	203.53	356	MAISAKA	34.68	137.62
60	HILO	19.73	204.93	362	NAGASAKI	32.73	129.87
61	MOKUOLOE	21.43	202.2	364	HAKODATE	41.78	140.73
71	WELLINGTON	-41.28	174.78	365	ISHIGAKI	24.33	124.15
79	CHATHAM	-43.95	183.43	370	MANILA	14.58	120.97
80	ANTOFAGASTA	-23.65	289.6	371	LEGASPI	13.15	123.75
81	VALPARAISO	-33.03	288.37	372	DAVAO	7.08	125.63
83	ARICA	-18.47	289.67	381	QUINHON	13.77	109.25
88	CALDERA	-27.07	289.17	382	SUBIC	14.82	120.28
91	LA	-2.2	279.08	383	VUNG	10.33	107.07
93	CALLAO	-12.05	282.85	417	SADENG	-8.5	110.78
94	MATARANI	-17	287.88	418	WAIKELO	-9.4	119.23

For latitudes, "-" denotes a site is located at the south of equator.

Table 1(B) (continue) Location information of 169 tide-gauge stations from GLOSS database

ID	Name	Latitude (°)	Longitude (°)	ID	Name	Latitude (°)	Longitude (°)
101	MOMBASA	-4.07	39.65	419	LAMBAR	-8.73	116.07
103	PORT	-20.15	57.5	420	MAUMLAKI	-7.98	131.28
104	DIEGO	-7.28	72.4	547	BARBERS	21.32	201.88
105	RODRIGUES	-19.67	63.42	548	KAUMALAPAU	20.78	203
108	HULHULE	4.18	73.53	551	SAN	37.8	237.53
109	GAN	0.68	73.15	552	KAWAIHAE	20.03	204.17
110	MUSCAT	23.63	58.57	554	LA	32.87	242.73
115	COLOMBO	6.97	79.87	556	CRESCENT	41.75	235.82

117	HANIMAADHOO	6.77	73.17	569	SAN	32.72	242.83
119	DJIBOUTI	11.6	43.15	592	SOUTH	44.63	235.95
121	POINT	-4.67	55.53	654	CURRIMAO	18.02	120.48
122	SIBOLGA	1.75	98.77	655	LUBANG	13.82	120.2
123	SABANG	5.83	95.33	684	PUERTO	41.48	287.03
124	CHITTAGONG	22.23	91.83	699	TANJONG	1.27	103.85
125	PRIGI	-8.28	111.73	702	LUDERITZ	-26.63	15.17
126	JASK	25.63	57.77	703	SALDAHNA	-33.02	17.95
128	THEVENARD	-32.15	133.63	704	CAPE	-34.18	18.43
129	PORTLAND	-38.35	141.6	708	SALVADOR	-12.97	321.48
142	LANGKAWI	6.43	99.75	729	MAR	-38.03	302.47
147	KARACHI	24.8	66.97	731	PUERTO	-42.77	294.97
149	LAMU	-2.27	40.9	737	SAN	12.58	278.3
155	DZAOUDZI	-12.78	45.25	738	SANTA	11.23	285.77
162	CILACAP	-7.75	109.02	739	EL	9.57	281.05
163	BENOA	-8.75	115.22	755	VIRGINIA	25.73	279.83
168	DARWIN	-12.47	130.85	762	PENSACOLA	30.4	272.78
171	COCOS	-12.12	96.9	775	GALVESTON(PIER21)29	29.32	265.2
175	FREMANTLE	-32.05	115.73	776	PUNTA	18.5	291.62
176	ESPERANCE	-33.87	121.9	777	PUERTO	19.8	289.3
181	DURBAN	-29.88	31	786	ROSEAU	15.3	298.6
184	PORT	-33.97	25.63	789	PRICKLEY	12	298.23
185	MOSSEL	-34.07	22.33	799	PORT	18.57	287.65
186	KNYSNA	-34.08	23.05	807	ALEXANDRIA	31.22	29.92
188	RICHARD'S	-28.78	32.1	824	MARSEILLE	43.3	5.35
207	CEUTA	35.9	354.68	830	LA	43.37	351.6
209	CASCAIS	38.7	350.58	878	BULLEN	12.18	290.98
211	PONTA	37.73	334.32	906	MOULMEIN	16.48	97.62
220	WALVIS	-22.95	14.5	907	SITTWE	11.68	92.77
221	SIMON'S	-34.18	18.43				

For latitudes, "-" denotes a site is located at the south of equator.

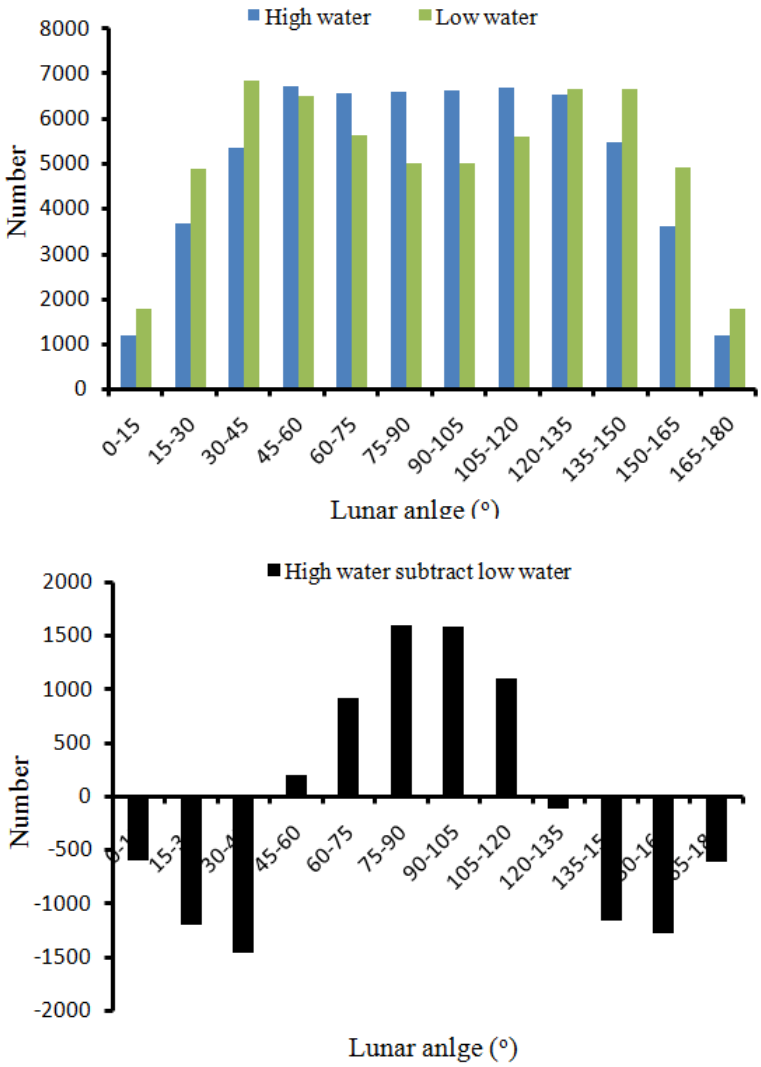

Figure 2. High and low water events of tide-gauge data out to lunar angle in 2014-08.

Another set of data is the sea surface height that was obtained from satellite altimetry. As tide-gauge stations are mostly located along coastlines and islands, tide-gauge data provide limited knowledge about the sea surface variation in the open ocean. Satellite altimetry provides a passage to overcome this shortcoming. More detail of satellite altimetry may refer to these works (Fu, et al, 2001; Fok, 2012). For oceans, satellite altimetry knows the sea surface height of a site relative to the reference ellipsoid at a time. Using this height to subtract the mean sea surface

height, we can obtain a sea surface variation of this site at the time. Theoretically speaking, if this variation is positive, it represents a high water behavior, and if the variation is negative, it represents a low water behavior. Altimetry data covering a period from 2014-08-01 05:57 to 2014-08-30 22:47 are selected from Jason-1 satellite of AVISO. The tracks of Jason-1 satellite may realize a global covering per 10 days, 30 days approximately represent 3 rounds of covering over the Earth's surface (Figure 3). To reduce the labor, we here select these data that are spanned with minute. Taking into account the Moon's position that transfers between 18°N and 18°S in the month, we use these sites that belong to a belt of 70°N and 70°S to do analysis. Satellite altimetry are influenced by various factors such as orbit error, atmospheric drag, radiation pressure, the tidal effects, satellite-originated thermal forces, and the measurement errors in various tacking systems (Fok, 2012). The tidal effects include ocean tides, solid Earth body tide, and pole tide. Before the usage of altimetry data, these influences must be exactly corrected. As ocean tides are represented with the equilibrium tide (i.e., the two bulges of water and the water depression), and because we are using sea level variation to examine the existence of the equilibrium tide, thus, the correction of ocean tides needs to be excluded. During this period, a total of 26901 sites are extracted from the dataset, the latitudes of these sites are actually between 66.15°N and 66.12°S. A statistical description of the number of high and low water events for these sites is shown in Figure 4. The high water events occur dominantly in the 45°-135° phases, while the low water events occur dominantly in the 0°-45° and 135°-180° phases. Of these sites, approximately 48.46% of the sites that fall into the 0°-45° and 135°-180° phases exhibit high water behavior, whereas approximately 40.13% of the sites that fall into the 45°-135° phase exhibit low water behavior. These results are in good agreement with the results obtained from tide-gauge data, tending to support that the two bulges of water and the water depression do not exist.

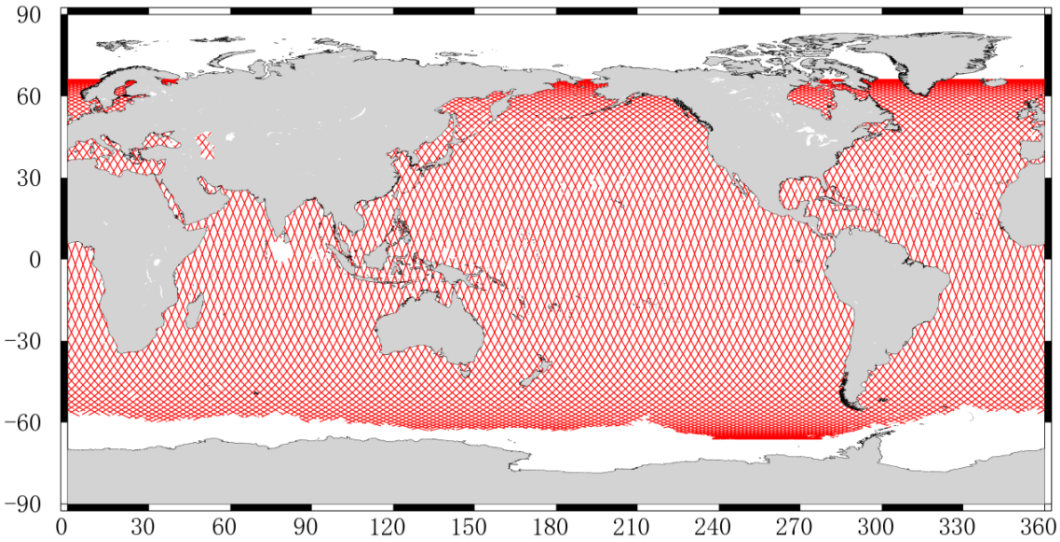

Figure 3. The ground tracks of Jason-1 satellite in cycle0027. The image of the tracks of Jason-1 satellite is provided by Dr. JiaJia Yuan/Shandong University of Science and Technology.

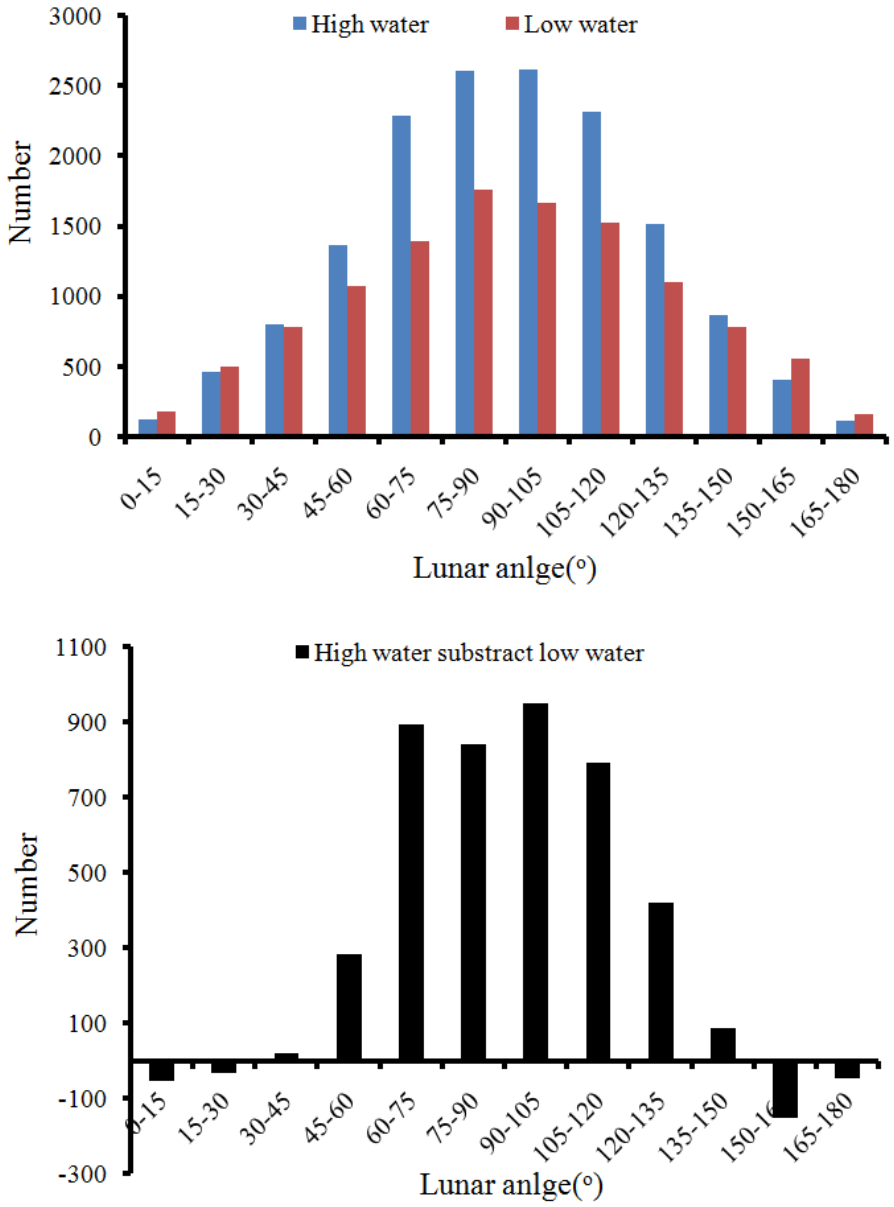

Figure 4. High and low water events of altimetry data out to lunar angle in 2014-08.

The dynamic tide theory begins with a consideration of the existences of water depth difference, landmass distribution, the Coriolis force, and friction, and with an assumption that the water's response to the gravitational forcing is slow, consequently, the observed tides are treated as a manifestation of the water movements that result from the complex ocean response to the forcing. The hydrodynamic equations and the ideas of wave are comprehensively used to describe the

water movements (Pugh, 1987; Pugh and Woodworth, 2014; Gerkema, 2019). This gives readers a sense that the observed tides are just the ones caused by the forcing, but the details of how the tides are initiated by the forcing remains elusive. The tractive force acting on a rotating watery Earth may be outlined with Figure 5(top). We assume at a special time that the Moon is located on the equator, five co-longitudinal water particles (i.e., *a*, *b*, *c*, *d*, and *e*) are put into the rightward tractive force and their initial speed is zero. The basic knowledge of physics allows us to accept that these particles are then driven by this force to accelerate towards the sub-lunar point (i.e., *m*). As the Earth spins from west to east, these moving particles finally exceed the sub-lunar point's longitude. From then on, these particles enter into the leftward tractive force, which is resistive, these particles then begin to decelerate. For the particles *a*, *b*, *d*, and *e*, given the tractive force exhibited in the left visible hemisphere represents the tractive force exhibited in the right invisible hemisphere, the movement directions of these four particles within the Earth's one rotation would traverse twice. If friction and obstacle are also neglected, these four particles would eventually pass the equator. On the whole, the water movement initiated by the tractive force in the northern (southern) hemisphere would move south-eastward (north-eastward) with a saw-like travelling path, while the water movement initiated by the tractive force on the equator would move eastward with a straight travelling path. Again, we assume at a special time that the Moon is located on the equator, these five co-longitudinal water particles are put into the leftward tractive force and their initial speed is zero. The result is the water movement initiated by the tractive force in the northern (southern) hemisphere would move south-westward (north-westward) with a saw-like travelling path, while the water movement initiated by the tractive force on the equator would move westward with a straight travelling path. And now we allow the Moon's declination to vary, the tractive force then swings longitudinally, this makes the water movement adjust accordingly. Further, friction and obstacle are included, friction would consume kinetics, this leads the travelling distance of the water movement to be less than the expectation; One obstacle is the water movement in the opposite direction that is initiated by the tractive force, another obstacle is the continents that would impede the water movement. One should be aware that it is particle movement to create wave other than wave to create particle movement. For instance, casting a little stone into a pond of water, the impact yields a pressure oscillation for the water, by which the water particles at the impacting site push adjacent water particles to move away, this outward movement of water particles behaves like wave. This

analysis leads to a point that the tidal waves initiated by the tractive force at the middle and high latitude hold not only longitudinal movement directed to the Earth-Moon line and but also latitudinal movement of either eastward or westward.

Figure 5(bottom) shows a map of the semidiurnal M_2 tides, which may be representatives of the observed tides around the world. Several features are evident here that the highest amplitudes occur mainly in the continental shelf seas, the co-tidal lines are approximately perpendicular to the coastlines, and most of oceans are marked with large amphidromic systems, in which the tidal phase performs a counterclockwise rotation in the northern hemisphere and a clockwise rotation in the southern hemisphere. These features are interpreted as that the tidal waves propagate from the deep oceans to the continental shelf seas, where they resonate with local oscillation and are also reflected/refracted by continents. Meanwhile, the Coriolis force deflects the moving tidal waves to the right in the northern hemisphere and to the left in the southern hemisphere (Pugh, 1987; Pugh and Woodworth, 2014).

We now assume the tidal waves initiated by the tractive force to move approximately westward and project them on the map of the semidiurnal M_2 tides. The tidal forcing continuously tracks from east to west, this fashion in principle allows the assumption above. It immediately becomes obvious that the propagation directions of the tidal waves initiated by the tractive force cannot be in accordance with the propagation directions of the tidal waves that are required for the tides at the middle and high latitudes. For example, to produce the tides (i.e., amphidromes) at the middle and high latitudes, the tidal waves initiated at the low latitude need to propagate towards the middle and high latitudes to interact, but the existing propagation directions are entirely opposed to this expectation. One should be aware that the Coriolis force doesn't do work, and it cannot reverse a southward (northward) moving tidal wave into a northward (southward) moving tidal wave.

Continents would reflect/refract the incoming tidal waves, but the existing propagation directions of the tidal waves are very difficult to be deflected to reach the middle and high latitudes. For the Pacific Ocean, its northwest boundary (i.e., Asian continent) is slightly tilt from south-west to north-east, the south-westward tidal waves would be reflected/refracted by this boundary to move roughly southward and impossible to move toward the northern ocean; The Philippines and Indonesia landmasses are located at the west of the ocean and are relatively sparse, the tidal waves reflected/refracted by them are difficult to reach the northern and southern ocean; The

Australian continent sits at the southwest of the ocean, the tidal waves reflected/refracted by this continent are also very difficult to reach the southern and northern ocean. For the Atlantic Ocean, the North Brazil is slightly tilt from south-east to north-west, the tidal waves refracted by this boundary are approximately directed to the Mexico and East America, and are difficult to make contribution to the tides in the northern Atlantic ocean; The travelling tidal waves initiated in the southern Indian Ocean may contribute to the tides in the southern Atlantic Ocean because of the connection between the two oceans, but they are very difficult to reach the northern Atlantic Ocean. For the enclosed regions such as the Red Sea, the south-westward moving tidal waves object to a counterclockwise rotation of the tides at this region.

Energetically speaking, the potential field represented by the tractive force is uniformly directed to the sub-lunar points (e.g., *m* and *m*'), the water particles at the middle and high latitudes trend to move along the force vector. With the continuous rotation of the cylindrical symmetric tractive force, all the water particles trend to be pulled to move from east to west, but an indisputable fact is the water particles at the middle and high latitudes trend to be pulled to move toward the low latitude. Apparently, the tides (i.e., amphidromes) at the middle and high latitudes prefer to a propagation of the tidal waves that are initiated at the low latitude, however, such a propagation is entirely fighting against the force vector. It is necessary to emphasize that in the horizontal momentum equation there is a term of $-(\Delta\Omega/\Delta x)$, as shown in the standard textbook (Pugh, 1987; Pugh and Woodworth, 2014), which denotes the direct tidal force, but this equation doesn't show how the tidal waves are initiated by the tractive force and how the tidal waves propagate from the lower latitude to the higher latitude. Another trouble with the gravitational forcing is that the Earth-Moon line is always swinging within the low latitude, mostly between 18^o N and 18^o S. The water particles at the middle and high latitudes are always pulled by the tractive force to move toward the low latitude, since the ocean water is conservative given water is incompressible and its density is constant, consequently, the water particles at the low latitude have to move back to the middle and high latitudes to compensate, this would require other force to do work overcoming the tractive force, but in practice we cannot find this other force. The image of the semidiurnal M_2 tides expresses a clear signal that the water exchange is not only latitudinal but also longitudinal, but under the control of the tractive force a longitudinal water exchange becomes impossible. Our argument of the water

movement under the tractive force and the observed tides suggests that the gravitational forcing cannot be realistic.

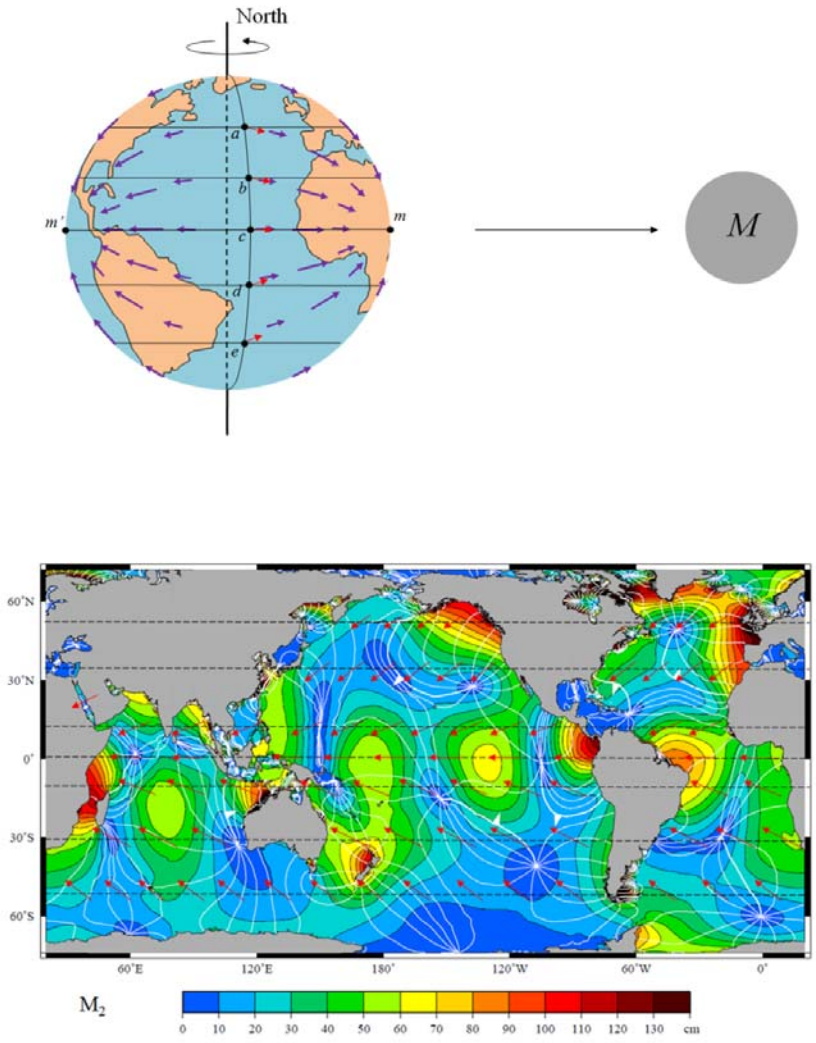

Figure 5. Model of water particle movement under the tractive force (top) and the semidiurnal M_2 tides distribution around the globe (bottom). Given the sub-lunar points (*m* and *m*') are located at the equator and the resulting tidal waves (marked with red arrows) under the tractive force (marked with purple arrows) are approximately westward. The image of M_2 tide is provided by Dr. Richard Ray/Space Geodesy branch, NASA/GSFC.

3 An oceanic basin oscillation-driving mechanism for tides

3.1 Water movement in an oscillating vessel

Our understanding of tides begins with a conceptual demonstration of water movement in an oscillating vessel. As shown in Figure 6, when the right end of a rectangular water box rises, the water then flows towards the left. If line MN represents a reference level, the water level at site M rises while the water level at site N falls. If we store the right end to its former level and raise the left end, then the water flows towards the right, the water level at site M falls, and the water level at site N rises. By repeating the rise and fall of the two ends continuously, the water level variations at sites M and N alternate. In contrast, site S, which is located in the middle of this vessel, always has a minimal water level change. In a view of energy transformation, the rising end of the vessel adds gravitationally potential energy to the water, when the end falls, the obtained potential energy is transformed into kinetic energy, as a result, the water moves. This demonstration suggests that an oscillating vessel may lead the water within it to move back and forth and further form an all-around water level change.

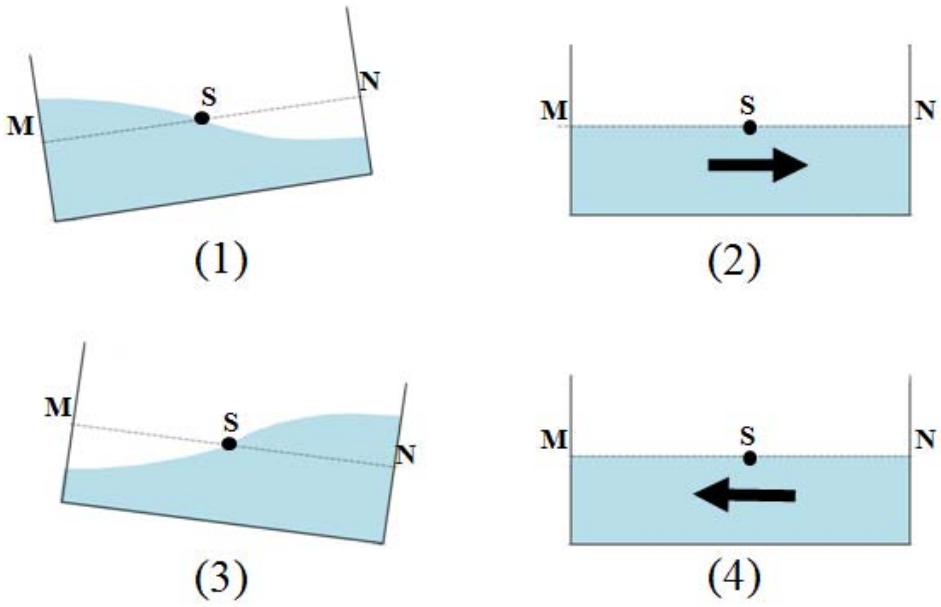

Figure 6. Modeling the water movement of an oscillating rectangular box. From (1), (2), (3) to (4),we observe an orderly representation of the full alternation of rise and fall at the two ends. Arrows denote the directions of water movement.

3.2 Solid Earth deformation

The Earth may be treated as a solid sphere that is enveloped by water and atmosphere Fowler, 2004; National Research Council, 1993). It has already been established that the Earth participates in two curved motions in space: one is the Earth orbiting around the center of mass of the Earth-Moon system and the other is the Earth-Moon system orbiting around the Sun. A fuller description of the motions of the Earth, Moon, and Sun may be found in these works (Kopal, 1969; Schureman, 1976; Smart, 1940; Doodson and Warburg, 1941; Kaula, 1968; Roy, 1978). Mechanically, these two curved motions can generate two centrifugal forces, F_1 and F_2, for a solid Earth (Fig. 7(a_1)). Note that these centrifugal forces are essentially inertia rather than real force. F_1 and F_2 can be counterbalanced by the centripetal forces, which are gravitation f_1 from the Moon and gravitation f_2 from the Sun, respectively. It is these force balances to make the Earth steadily move around the enter of mass of the Earth-Moon system and around the Sun. If we use the established parameters (e.g., orbital radius, orbital period, and mass of each body) for this estimation, then F_2 would be far greater than F_1. Since the working point of F_2 is not located at the Earth's center, we assume that the effective part of F_2, which enables stretching of the Earth's body, to be relatively small and exerted at the Earth's center. The solid Earth is not strictly a rigid body, its elastic response to a combination of these two opposing forces F_1 (F_2) and f_1 (f_2) finally elongates its body along the Earth-Moon (Sun) line and compresses the body in the midway of the elongation. The combined force could be the tide-generating force that is a difference between the gravitational force and the centrifugal force. The net effect of the response is that the solid Earth becomes an oblate spheroid (Fig. 7(a_2 and a_4)). We refer to these actions as lunar (solar) deformations in the following sections. The deformation of a solid sphere that runs along a curved path can be illustrated with Figure 6(a_6). The sphere is entrained by a rod to rotate, and the curved motion yields a centrifugal force f, which can be written as $f=Mv^2/r$, where M, v, and r are respectively the mass, speed, and orbital radius of the sphere, respectively. The centrifugal force f is counterbalanced by a centripetal force F, which is essentially a pull force that is exerted along the rod, and $F=f$. Under the interaction of pull force F and centrifugal force f, the sphere is elongated along the line of force.

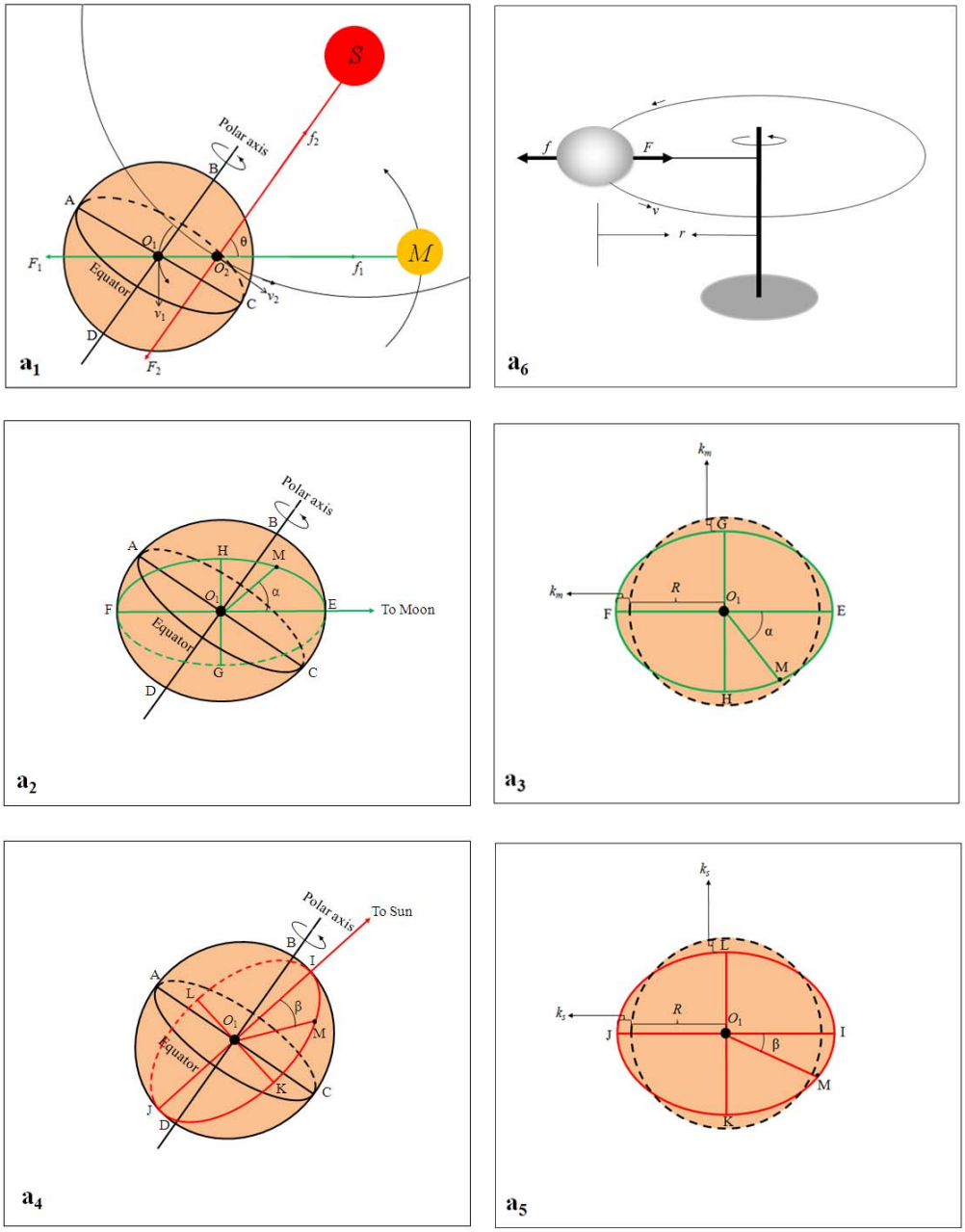

Figure 7. Combined centrifugal effects for the solid Earth and the resultant deformation.a_1 represents the curved motions of the Earth around the barycenter of the Earth-Moon system and around the Sun; a_2 and a_4 are the resultant deformations due to the Moon and Sun; a_3 and a_5 are the sections dissected from these deformations; a_6 demonstrates how a sphere is deformed under the effect of pull force and centrifugal force; F_1 and F_2 are the centrifugal effects undergone by the solid Earth in these curved motions; O_1, O_2, M, and S are the Earth's center, the barycenter of

the Earth-Moon system, the Moon, and the Sun, respectively; Θ is the angle of the Moon and Sun relative to the barycenter of the Earth-Moon system; and v_1 and v_2 are the velocity of the Earth orbiting the barycenter of the Earth-Moon system and the velocity of the Earth-Moon system orbiting the Sun, respectively. The black dashed circles in diagrams a_3 and a_5 denote the original shape of the solid Earth.

Solid Earth deformation can be influenced by several factors. Near-surface geology yields local anomalies under the gravitational forcing. The loading/unloading of ocean tides results in a change of gravity and a redistribution of the ocean's weight, as a response to these adjustments, the lithosphere moves vertically and tilts (Pugh, 1987; Farrell, 1973). Additionally, atmospheric loading and some extreme events (such as a storm or earthquake) can also exert effect on the Earth's lithosphere. However, these influences are either local or trivial when solid Earth deformation under the gravitational forcing is treated as a whole, they may be ignored.
Solid Earth deformation (often called Earth tide) have been extensively discussed (Agnew, 1981; Pugh and Woodworth, 2014; Gerkema, 2019), and its amplitude is calculated through the potential equations. Different from this routine, we here assume the deformation has been yielded by the external forces and only use a least-square fitting to constrain its amplitude. Since the near side of solid Earth undergoes more Moon's gravitational attraction than its far side does, the tide-generating force at the near side is therefore greater than tide-generating force at the far side, the response of solid Earth to these unequal forces is to yield an asymmetrically oblate spheroid. To expedite the following deduction, we ignore the asymmetry. Geometrically, a section that cuts an oblate spheroid along its long axis must be an ellipse (Fig. 7(a_3 and a_5)); then, the displacement of an Earthly site (marked with M) relative to the Earth's center at time t may be expressed as follows:

$$\Delta Y_{(t)}=\Delta H(lunar)_{(t)}+\Delta H(solar)_{(t)} \quad (1)$$

$$\Delta H(lunar)_{(t)}=[(R+k_m)^2\cos^2\alpha+(R-k_m)^2\sin^2\alpha]^{1/2}-R$$

$$\Delta H(solar)_{(t)}=[(R+k_s)^2\cos^2\beta+(R-k_s)^2\sin^2\beta]^{1/2}-R$$

where $\Delta H(lunar)_{(t)}$ and $\Delta H(solar)_{(t)}$ are the displacements of site M in the lunar and solar deformations, respectively, R is the mean radius of the solid Earth, k_m and k_s are the amplitudes of the lunar and solar deformations, respectively, and α and β are the lunar and solar angles of site M. The angles may be obtained through the following formulas of spherical geometry:

$\cos\alpha=\sin\sigma\sin\delta_m+\cos\sigma\cos\delta_m\cos C_{mm}$ and $\cos\beta=\sin\sigma\sin\delta_s+\cos\sigma\cos\delta_s\cos C_{ms}$, where σ, δ_m, δ_s, C_{mm}, and C_{ms} are the geographic latitude of site M, the declination of the Moon, the declination of the Sun, the hour angle of site M with respect to the Moon, and the hour angle of site M with respect to the Sun, respectively.

Equation (1) indicates that an Earthly site would periodically rise and fall as the elongated solid Earth spins around its axis and that the amplitude of the rise and fall would vary with the positional adjustments of the Moon, Sun, and Earth in space. In particular, this amplitude reaches the maximum at the full Moon and new Moon and a minimum at the first quarter and last quarter because at the full and new Moon, the two sets of deformations are added to reinforce each other, whereas during the first quarter and last quarter, the two cancel each other out and weaken. The amplitude $k_m(k_s)$ can be obtained by resolving a relationship between gravity and lunar angles. Gravitational acceleration of an Earthly site fits the relationship of $g_H=GMe/H^2$, and the resultant gravity change may be expressed as $\Delta g=(1/H^2-1/R^2)GMe$, where G, Me, R, and H are the gravitation constant, mass of the Earth, mean radius of the Earth, and the distance of an Earthly site from the Earth's center, respectively. Based on Equation (1), the distance may be written as $D=((R+k_m)^2\cos^2\alpha+(R-k_m)^2\sin^2\alpha)^{1/2}+((R+k_s)^2\cos^2\beta+(R-k_s)^2\sin^2\beta)^{1/2}-R$. A purely experienced expression for these two deformations may be written as $k_m=E_mQ_m(\cos\delta_m+\cos\Theta)$ and $k_s=Q_s\cos\delta_s$, where E_m is the elliptical coefficient of the Moon's orbit and may be further written as $E_m=R_{ME}^2/R_M^2$ (R_{ME} and R_M are the mean distance of the Moon from the Earth and the Moon's orbital radius, respectively); Q_m and Q_s denote the amplitude of the lunar and solar deformations, respectively; and δ_m, Θ, and δ_s denote the Moon's declination, the angle between the Moon and Sun, and the Sun's declination, respectively. After these parameters are determined, we employ the hourly gravity data of 4 sites from IGETS (International Geodynamics and Earth Tide Service) (Voigt et al., 2016) via a least-squares fitting to resolve Q_m and Q_s. The time span lasts from 2014/08/01 to 2014/08/30. Since each gravity gauge site has its own reference level g_{re}, the gravity change of a site may thus be expressed as $\Delta g=(1/H^2-1/R^2)GMe-g_{re}$. The related parameters (G, Me, R, and R_{ME}, for example) bearing these calculations and the results of Q_m, Q_s, and g_{re} are listed in Table 2.

Table 2 Parameters and results for lunar and solar deformations

Gravity gauge Station	Apache Point	Bad Homburg	Canberra	Sutherland	Mean
Q_m (m)	0.19	0.18	0.19	0.19	0.19
Q_s (m)	0.11	0.12	0.11	0.11	0.11
g_{re} (nm/s^2)	379.04	695.91	426.76	371.88	--
Astronomical parameters	Moon	M_m	$7.35*10^{22}$ kg (Wieczorek et al., 2006)		
		R_{ME}	384,400 km (Wieczorek et al., 2006)		
	Earth	M_e	$5.97*10^{24}$ kg (Luzum et al., 2011)		
		R	6370 km (Lide, 2000)		
	Sun	R_s	$1.49*10^{8}$ km (Simon et al., 1994)		
		M_s	$1.99*10^{30}$ kg (Williams, 2013)		
	G		6.67×10^{-11} m^1 s^{-2}		

Note: Q_m, Q_s, and g_{re} are the amplitude of the lunar and solar deformations and gravity reference level of each site, respectively; M_m, M_e, and M_s are the Moon's, the Earth's, and the Sun's mass, respectively; R is the Earth's mean radius, R_{ME} and R_s are the mean distance of the Moon from the Earth and the mean distance of the Sun from the Earth, respectively; and G is a gravitational constant.

The elongated solid Earth would require an Earthly site to move up and down as the Earth spins. The rise (fall) of a site results in a fall (rise) of gravity; thus, gravity changes may be an index to examine the existence of these bulges of the solid Earth. Temporal gravity changes have been measured for decades, and an internationally cooperative network IGETS was established to provide gravity data. These measurements of temporal gravity are presently limited to continents, which leads to a lack of coverage for ocean basins. The rise (fall) of a site in the ocean floor would lead water to flow, and the water depth change may lead to variations in bottom pressure; thus, bottom pressure data may be second index to examine the existence of these bulges of the solid Earth.

The hourly gravity data of 12 sites from IGETS that cover three time spans (2012/01, 2014/08, and 2016/12) are employed (Voigt et al., 2016). At present, more than 40 gravity gauge stations are included in the IGETS network, with most located in Europe and the remaining stations scattered around other continents. We believe that the 12 selected sites may represent all gravity gauge stations. Gravity changes at the selected 12 sites and their lunar angles are compared in Figure 8. These sites uniformly show a decrease in gravity when their lunar angles fall into a phase of 0°~45° and 135°~180°, whereas they uniformly show an increase in gravity when their lunar angles fall into a phase of 45°~135°.

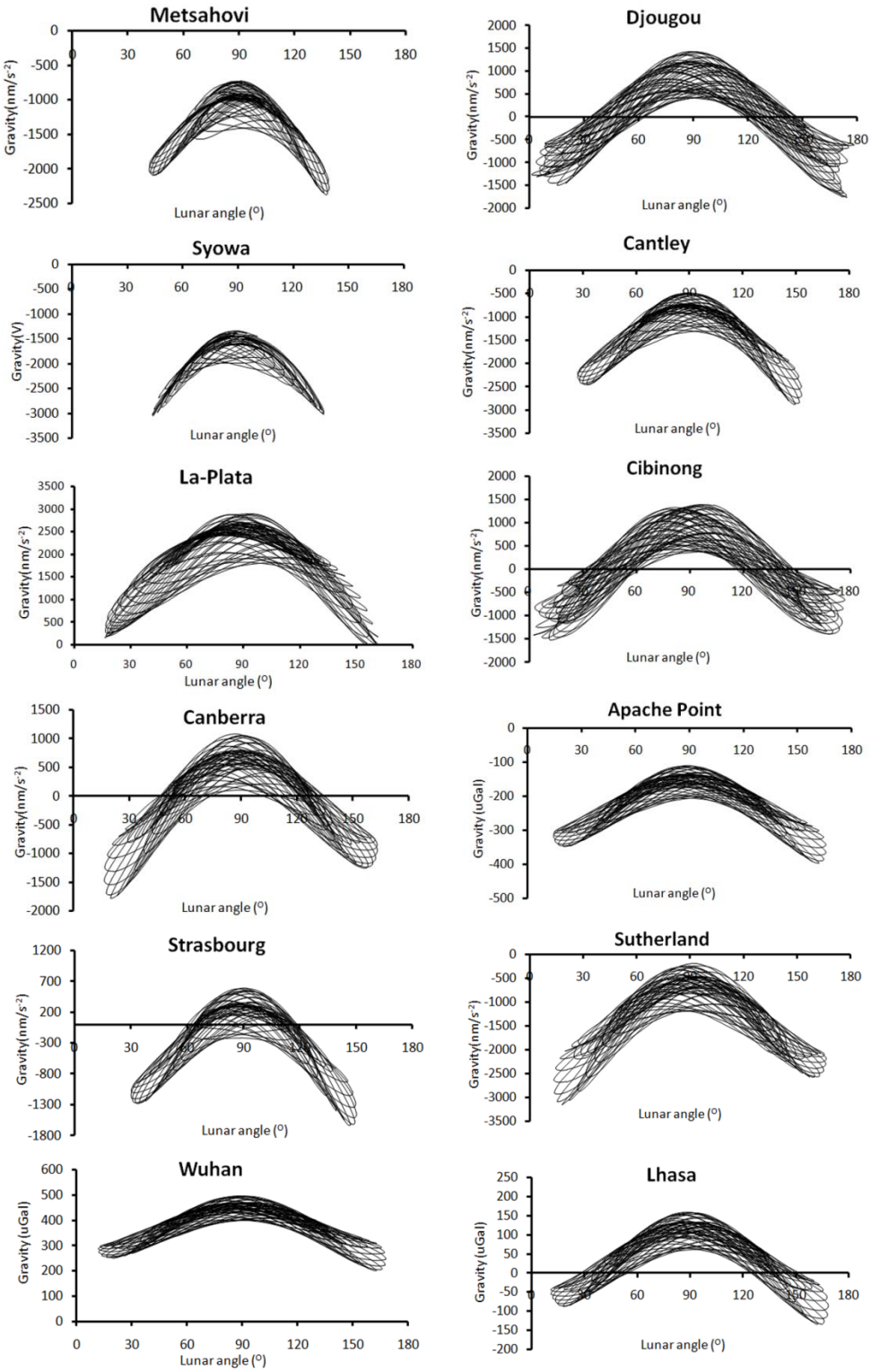

Figure 8. Solid Earth deformation versus gravity change. Hourly gravity data are extracted from IGETS (Voigt et al., 2016).

The hourly bottom pressure data from 32 sites that mostly cover August 2014 are selected from the NOAA NDBC (National Oceanic and Atmospheric Administration National Data Buoy Center). There are more than 70 bottom pressure gauge stations included in the network of the NDBC. To some extent, the 32 selected sites may be representative of all bottom pressure gauge stations. A geographic distribution of the 12 selected gravity and 32 bottom pressure gauge sites is shown in Figure 9. The bottom pressure of the 32 sites and their lunar angles are compared in Figure 10. The geographical positions of these gauge sites and their data span are further listed in Table 3. Unlike the relationship between gravity change and lunar angle, which is steadily uniform, the relationship between bottom pressure change and lunar angle becomes relatively complicated. Of these 32 sites, 16 sites orderly show a decrease in pressure when their lunar angles fall into the phases of 0°~45° and 135°~180°, and an increase in pressure when their lunar angles fall into the phase of 45°~135°; 8 sites orderly show a rise in pressure when their lunar angles fall into the phases of 0°~45° and 135°~180°, and a decrease in pressure when their lunar angles fall into the phase of 45°~135°; and the remaining 8 sites remain disordered. This situation may occur because the response of water to basin oscillations is too complicated. For example, the outflow of water at a rising site would result in an inflow of water towards another site, and the inflow of water may offset the outflow of water at another site that is generated due to basin oscillation. Overall, the dominant pattern of the relationship between bottom pressure and lunar angle tends to follow that of gravity change and lunar angle. Because these gauge stations are extensively distributed around the globe, their close response to lunar angle under gravity change and bottom pressure change provides evidence for the existence of two solid bulges. Although gravity field measurements have been globally obtained by satellites, the resultant data are not temporal and therefore cannot be used in this work. Technical progress is required in the future to measure temporal gravity changes in the ocean floor and obtain a better understanding of ocean basin deformation.

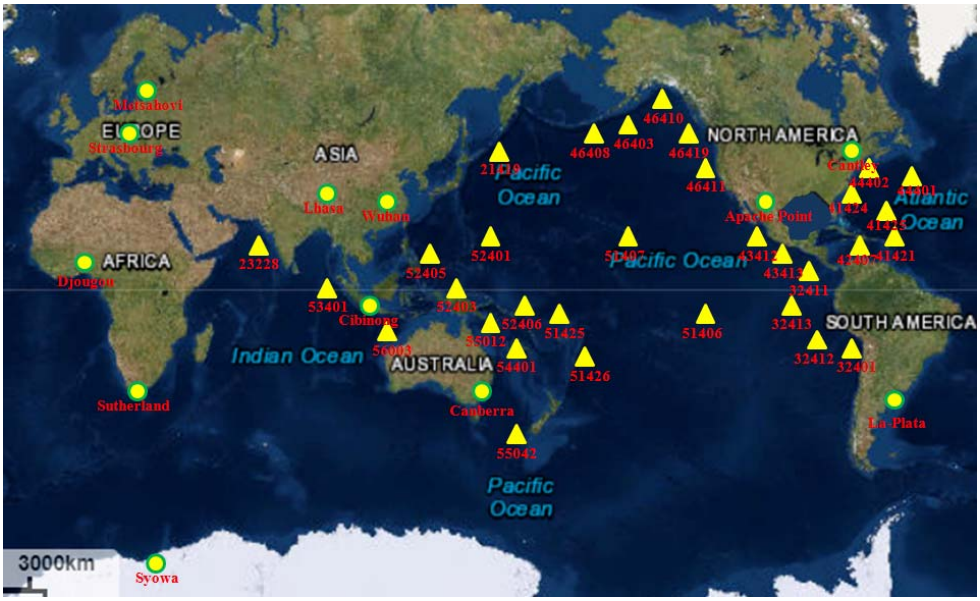

Figure 9. Geographic distribution of the 12 selected gravity sites and 32 bottom pressure gauge sites. Yellow triangles denote bottom pressure gauge sites, while green circles denote gravity gauge sites. The background is from Earthstar Geographic.

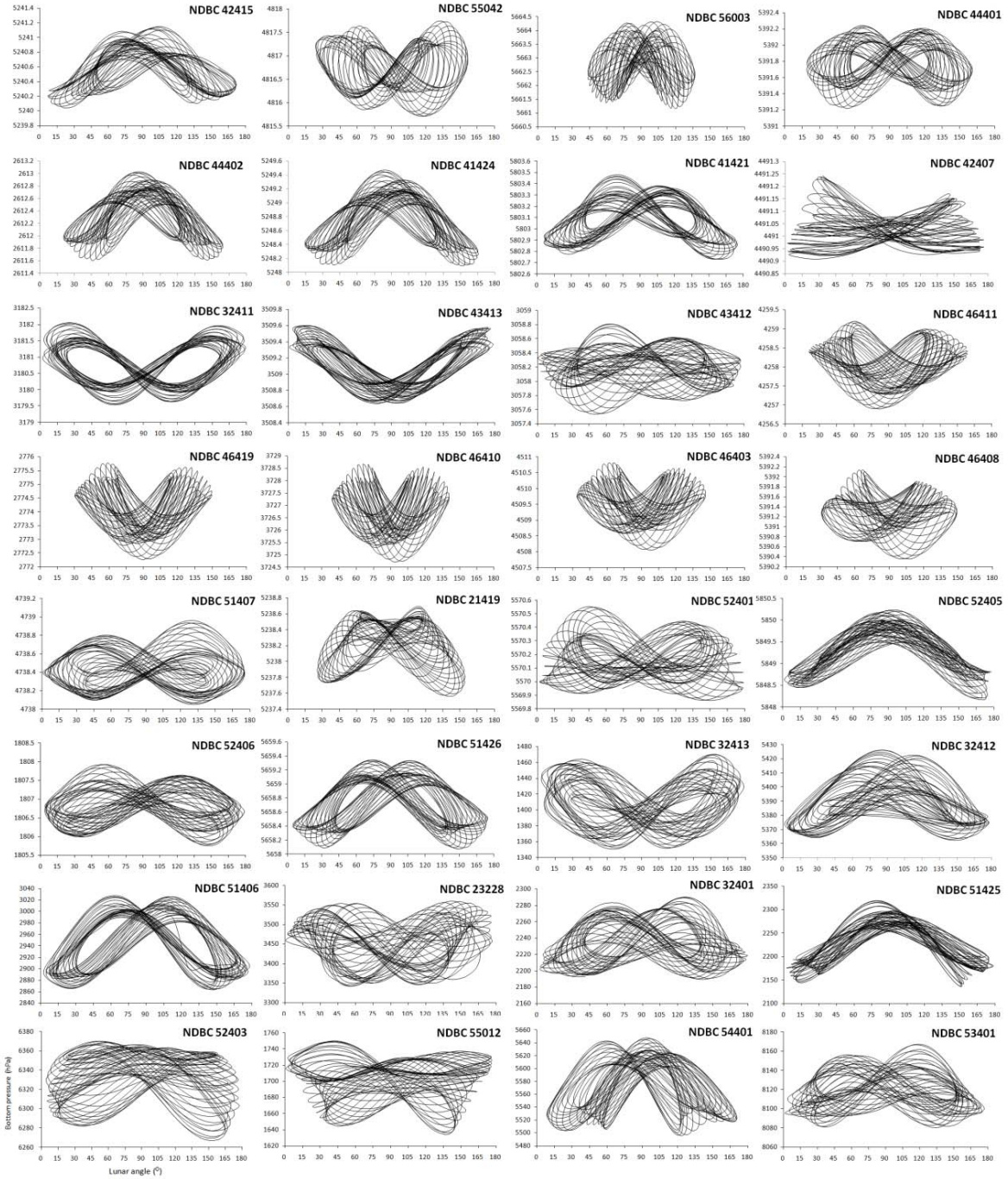

Figure 10. Solid Earth deformation versus bottom pressure change. Hourly bottom data were extracted from National Oceanic and Atmospheric Administration National Data Buoy.

Table 3(A) Geographic location and data span for 32 bottom pressure (gravity) gauge sites

Data type	Location name	Latitude (°)	Longitude (°)	Time
Bottom pressure	NDBC 41425-Southwest Bermuda	28.63	294.35	2019/02/01-2019/02/28
	NDBC 55042-Tasman Sea 2	-44.90	161.84	2019/02/01-2019/02/28
	NDBC 56003-Indian Ocean 2	-15.02	117.94	2014/08/01-2014/08/30
	NDBC 44401-Northeast Castle Rock Seamount	37.59	309.97	2014/08/01-2014/08/30
	NDBC 44402-Southeast Block Canyon	39.30	289.34	2014/08/01-2014/08/30
	NDBC 41424-East Charleston	33.00	287.34	2014/08/01-2014/08/30
	NDBC 41421-North St Thomas	23.41	296.22	2014/08/01-2014/08/30
	NDBC 42407-South Puerto Rico	15.29	291.81	2014/08/01-2014/08/30
	NDBC 32411-West Panama	4.59	269.12	2014/08/01-2014/08/30
	NDBC 43413-South Acapulco	11.01	259.92	2014/08/01-2014/08/30
	NDBC 43412-Southwest Manzanillo	16.05	253.03	2014/08/01-2014/08/30
	NDBC 46411-Mendocino	39.33	232.93	2014/08/01-2014/08/30
	NDBC 46419-Northwest Seattle	48.80	230.38	2014/08/01-2014/08/30
	NDBC 46410-South Cordova	57.65	216.22	2014/08/01-2014/08/30
	NDBC 46403-Southeast Shumagin Island	52.67	203.04	2014/08/01-2014/08/30
	NDBC 46408-Nikolski	49.66	190.10	2014/08/01-2014/08/30
	NDBC 51407-Hawaii	19.55	203.46	2014/08/01-2014/08/30
	NDBC 21419-Kuril Islands	44.44	155.72	2014/08/01-2014/08/30
	NDBC 52401-Northeast Saipan	19.26	155.75	2014/08/01-2014/08/30
	NDBC 52405-South Philippine Sea	13.04	132.16	2014/08/01-2014/08/30

	NDBC 52406-Northeast Solomon	-5.33	165.03	2014/08/01-2014/08/30

Note: Interpolations are performed for the these bottom pressure sites: 56003,46411,46419, 46403, 51407, 51406, 23228, and 51425. Bottom pressure data are selected from the NOAA NDBC and PSMSL (Permanent Service for Mean Sea Level), and gravity data are selected from the IGETS. For latitudes, "-" denotes a site is located at the south of equator.

Table 3(B) (continue) Geographic location and data span for 44 bottom pressure (gravity) gauge sites

Data type	Location name	Latitude (°)	Longitude (°)	Time
Bottom pressure	NDBC 51426-Southeast Tonga	-23.11	191.62	2014/08/01-2014/08/30
	NDBC 32413-North West Lima	-7.40	266.50	2012/02/22-2012/03/22
	NDBC 32412-South West Lima	-17.98	273.66	2012/02/22-2012/03/22
	NDBC 51406-Central South Pacific	-8.48	234.97	2012/02/22-2012/03/22
	NDBC 23228-Arabian Sea	20.80	65.35	2013/02/26-2013/02/27
	NDBC 32401-260 NM WSW of Arica, Chile	-20.47	286.57	2013/02/26-2013/02/27
	NDBC 51425-North West Apia	-9.51	183.76	2013/11/26-2013//11/25
	NDBC 52403-North Manus	4.05	145.62	2013/11/26-2013//11/25
	NDBC 55012-Coral Sea 1	-15.80	158.40	2013/11/26-2013//11/25
	NDBC 54401-North East New Zealand	-33.02	187.04	2010/10/04-2010/11/02
	NDBC 53401-Indonesia	0.05	91.90	2007/10/08-2007/11/04
Gravity	Canberra, Australia	-35.32	149.01	2014/08/01-2014/08/30
	Apache Point, USA	32.78	254.18	2014/08/01-2014/08/30
	Sutherland, South Africa	-32.38	20.81	2014/08/01-2014/08/30
	Djougou, Benin	9.74	1.61	2014/08/01-2014/08/30
	Strasbourg, France	48.62	7.68	2014/08/03-2014/08/30

Lhasa, China	29.65	91.04	2014/08/01-2014/08/30
Wuhan, China	30.52	114.49	2014/08/01-2014/08/30
Cibinong, Indonesia	-6.49	106.85	2012/01/01-2012/01/31
Metsahovi, Finland	60.22	24.40	2014/08/01-2014/08/30
Cantley, Canada	45.59	284.19	2014/08/01-2014/08/30
Syowa, Antarctica	-69.01	39.60	2002/12/01-2002/12/31
La-Plata, Argentina	-34.87	301.86	2016/12/01-2016/12/31

Note: Interpolations are performed for the these bottom pressure sites: 56003,46411,46419, 46403, 51407, 51406, 23228, and 51425. Bottom pressure data are selected from the NOAA NDBC and PSMSL (Permanent Service for Mean Sea Level), and gravity data are selected from the IGETS. For latitudes, "-" denotes a site is located at the south of equator.

Approximately 71% of the Earth's surface is covered with ocean (Pidwirny, 2006), the elongated solid Earth would require ocean water to mechanically flow towards the depression that is midway along the elongated body, a concentration of water would form a weak ring of water on the Earth's surface. The frame of the two solid bulges and a ring of water is outlined in Figure 11. Areas *a-cdef* and *b-ghij* represent the two bulging solid regions, while area *cdef-ghij* represents the water ring. It may be expected that an Earthly site (marked with *S*, for instance) falling into these bulges of solid Earth would exhibit low water behavior while an Earthly site falling into the water ring would exhibit high water behavior. Geometrically speaking, when an Earthly site's lunar angle falls into a phase of 0°~45° or 135°~180°, it indicates this site enters into one of the two bulges of solid Earth, and when the lunar angle falls into a phase of 45°~135°, it indicates this site enters into the water ring. The results of both tide-gauge and satellite altimetry data are employed again. It has been shown in Figure 2 and Figure 4, the high water events occur dominantly in the 45°-135° phase, while the low water events occur dominantly in the 0°-45° and 135°-180° phases. These results tend to agree with the existence of the two bulges of solid Earth and the water ring.

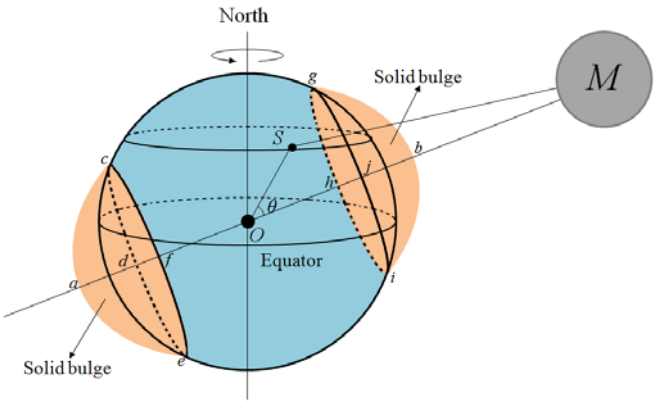

Figure 11. Model of Earth's two solid bulges and the Moon in space. *O* and *M* denote the Earth's center and the Moon, respectively. *θ* is the lunar angle of an Earthly site (marked with *S*). Note that the two solid bulges are highly exaggerated in this figure.

3.3 The elongated spinning of solid Earth and its resultant tides

The elongated spinning of solid Earth leads to oscillations in each part of the ocean basin. As shown in Figure 12(A and B), the two bulges of solid Earth in the lunar deformation track from

east to west along lines *L* and *L'*, which leads each part of the ocean basin to move up and down. The ocean basin is a naturally gigantic container of water, thus, the oscillation of the basin leads the water within it to mechanically flow. The reason for the water movement will be discussed later. Since the ocean basin is successively shaken by the two solid bulges, the water movement occurs regularly, the ocean surface then obtains two high and two low water levels per day; Due to the disturbance of the landmass and the Earth's rotation, each part of the ocean surface is unnecessary to strictly occur two high and two low water levels per day; In some of the extreme cases, there would occur one high and one low water levels per day. In most time, the two solid bulges are located on the two sides of the equator, this leads to differences in the two shakes of the ocean basin, and further leads to unequal amplitudes for the two high or low waters per day. In particular, when the ocean basin oscillation generated due to the lunar deformation is associated with the ocean basin oscillation generated due to the solar deformation, a combination of two sets of oscillations would make water movement become strongest during full and new Moons and become weakest during the first quarter and last quarter. This interaction generates two cycles of high and low water levels over the course of a month (Figure 13).

Plotting the two solid bulges on the map of the semidiurnal M_2 tides, and in consideration of the water movement in the oscillating vessel in section 3.1, it becomes obvious that that the propagation directions of the water movements initiated by the double solid bulge can be in accordance with the propagation directions of the water movements that are required for the observed tides (Figure 12(C)). For example, one solid bulge raises the eastern part of the Pacific ocean basin, the raising part makes the water move radically. One of the water movements propagates north-westward, because of the deflection made by the Coriolis force and the reflection/refraction made by the continent, this fits to the amphidromic system at the northern Pacific Ocean. Some of the water movements propagate south-westward, this fits to the amphidromic system at the northern Pacific Ocean. Others of the water movements propagate westward, this fits to those tides at the west. At the same time, another solid bulge raises the northeast part of the Indian ocean basin, the resulting water movements fit to the amphidromic systems at this region. One can imagine that, with the passage of time, one solid bulge would arrive in the middle of the Pacific ocean basin, at the moment some of the south-westward water movements would be refracted by the eastern part of the Australian continent, together with the aid of the Coriolis force, a counterclockwise amphidromic system may be formed, as that

amphidrome around the New Zealand. And when one of the two solid bulges moves to the middle of the Atlantic ocean basin, some of the water movements propagate northward, together with the aid of the Coriolis force, the amphidromic system at the northern Atlantic ocean may be formed. Meanwhile, part of the water movements propagate southward, they subsequently interact with the water movements propagated from the Indian Ocean, this fits to the two amphidromic systems at the southern Atlantic ocean. After the double solid bulge passes, the raised part of the basin falls naturally, this would induce a returning water movement, by which the conservation of water is realized. Certainly, the tracking double solid bulge would shake the enclosed sea basins, too. For example, when one solid bulge sweeps the Red Sea basin, the southeast part of the basin is firstly raised, this leads the water to move north-westward, together with the aid of the Coriolis force and the refraction, this fits to the amphidromic system at this region. So do for the amphidromic systems at the Mediterranean Sea. Comparing Figure 5 with Figure 12, we can easily determine which of the two mechanisms (i.e., the gravitational forcing and ocean basin oscillation) is the best way for the initiation of the water movement.

The hydrodynamic equations of continuity and momentum and the theoretical ideas of wave are successful in describing the water movements in the ocean basins and in select areas. To connect the ocean basin oscillation to these established understandings, we need to make two corrections: 1) the horizontal momentum equation includes a term of $-(\Delta\Omega/\Delta x)$, which denotes the direct tidal force (i.e., the tractive force). We here replace this force with a push force that is exerted by the solid bulge on the water, and then $\Delta\Omega$ denotes the work done by the solid bulge along the horizontal distance Δx. 2) two sets of tidal waves, represented by the lunar deformation and the solar deformation, are allowed to propagate in the ocean basins.

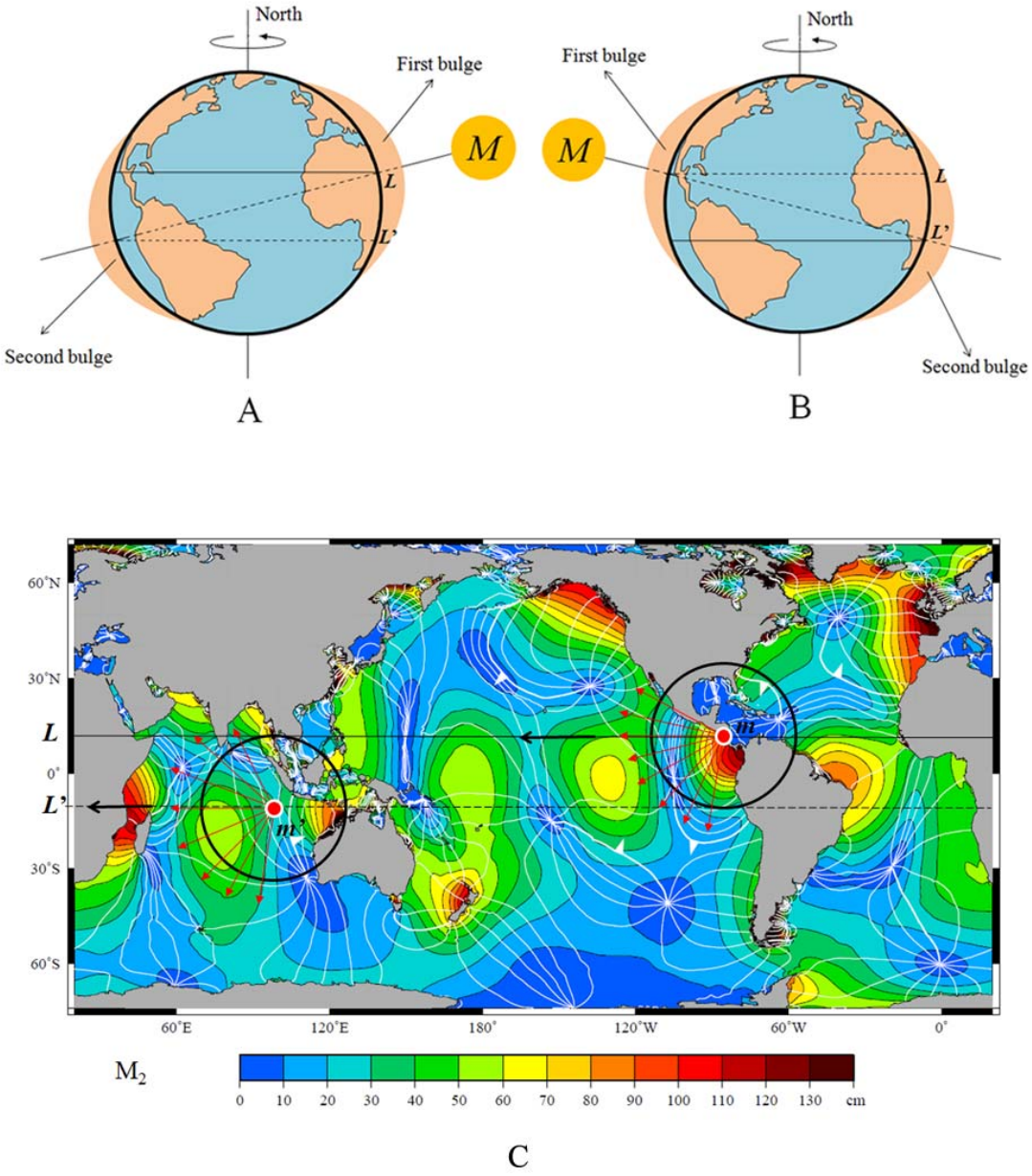

Figure 12. Model of the spinning elongated solid Earth and the resultant water movements. From A to B, the Earth rotates 180° with respect to the Moon. *L* and *L'* denote the paths that the Earth-Moon line tracks along the Earth's surface (dashed line means the track is at the far side), and the two bulges represent elongation of the solid Earth. In C, the solid bulges (black circle)

are plotted on the image of the M_2 tide in order to express the resulting water movements. The image of M_2 tide is provided by Dr. Richard Ray/Space Geodesy branch, NASA/GSFC.

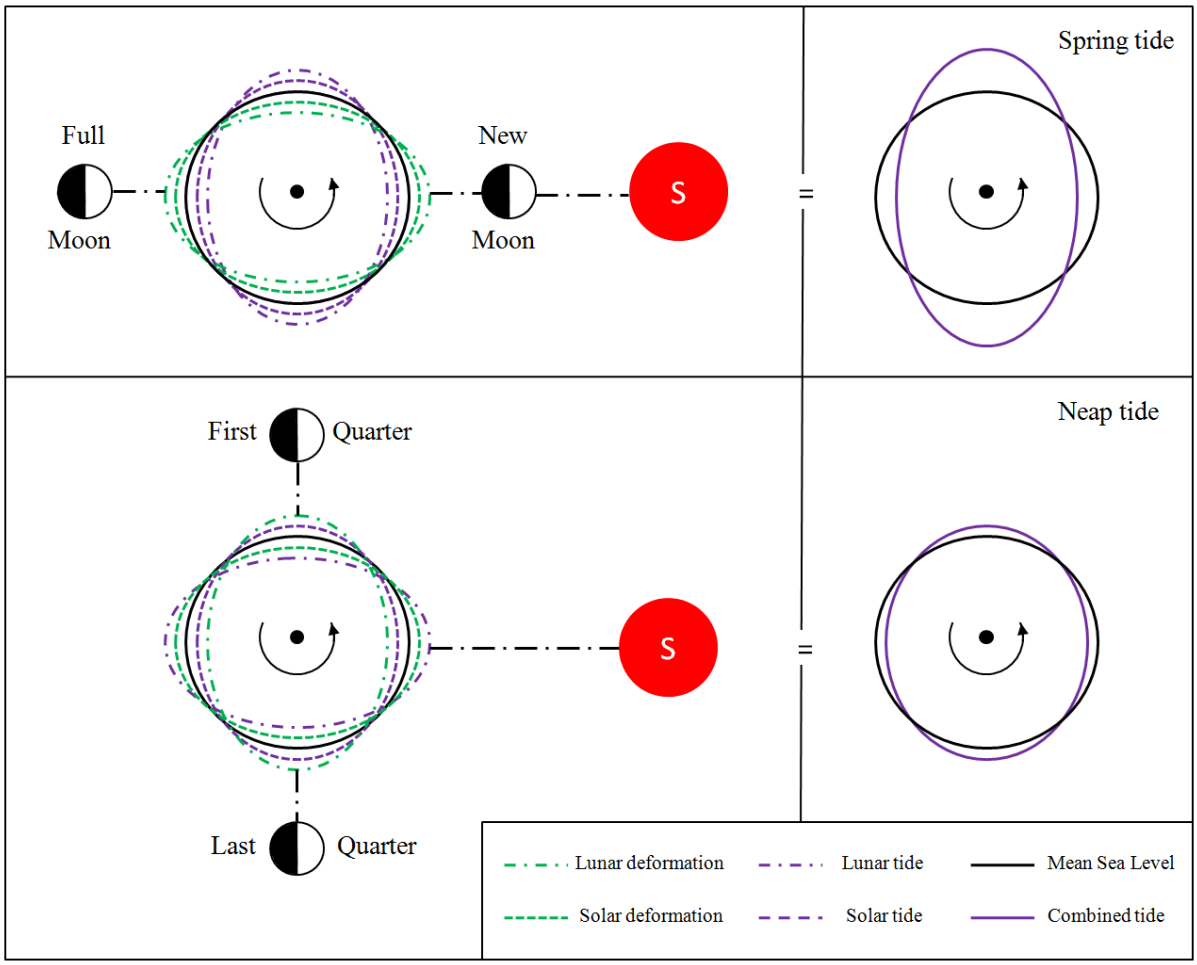

Figure 13. Modelling the Sprin-Neap tides under the relative motions of the Moon and Sun. The lunar deformation and solar deformation combine to produce spring tides at the new and full Moon and neap tides at the Moon's first and last quarter. Lunar deformation denotes the solid Earth deformation caused by the Moon's gravitational force, while solar deformation does the solid Earth deformation caused by the Sun's gravitational force. Lunar tide denotes the ocean tide caused by the lunar deformation, while solar tide does the ocean tide caused by the solar deformation. Note the sketch is highly exaggerated.

3.4 Predicting tides

The demonstration above indicates how water moves in an oscillating ocean basin, although the reason why water can move in the basin remains unresolved and deserves a discussion. As shown in Figure 14(top), the rising part of the ocean basin instantly raises the water above it while the falling part instantly decreases the water above it; consequently, the gravitational potential of the ocean surface varies everywhere. For example, the potential of site A decreases while the potential of site B increases. Ocean water is not only liquid but also continuous, its potential represents pressure. Under the effect of this pressure difference, water begins to move horizontally.

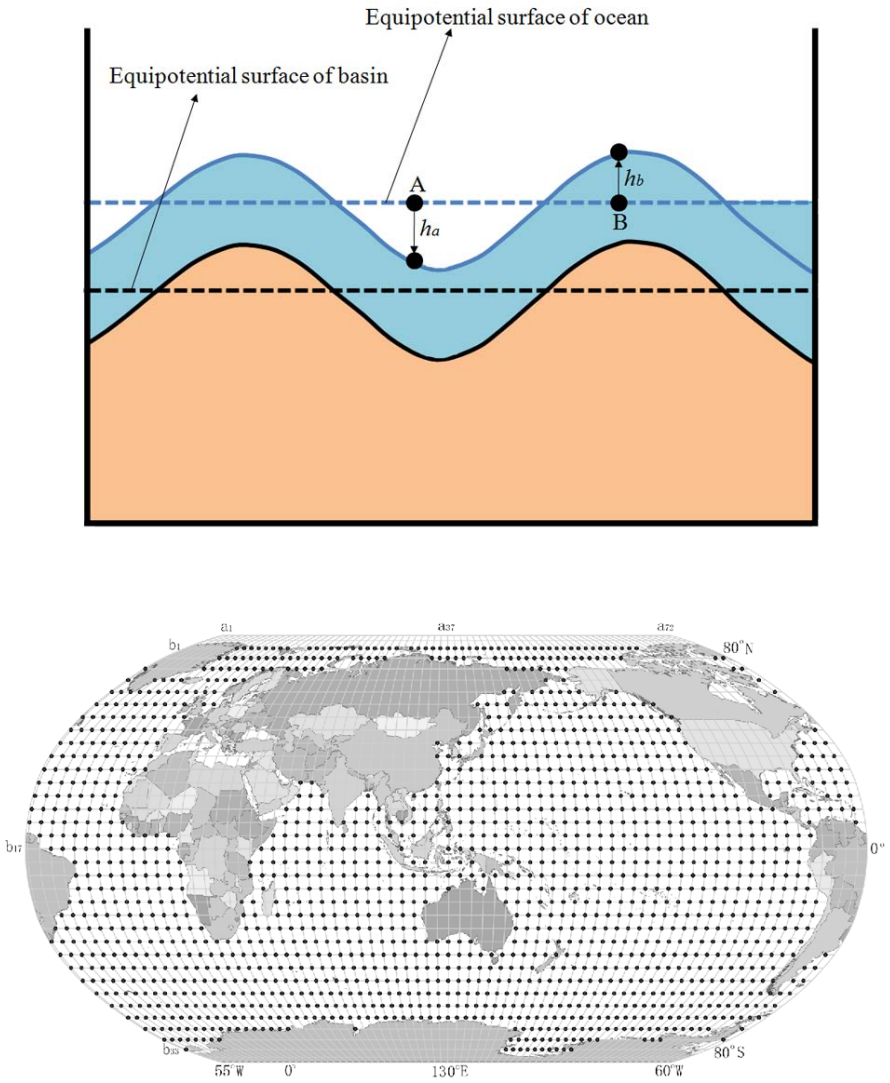

Figure 14. (top) Model of instant adjustments of ocean and basin during lunar deformation. Note that the deformations of both the ocean and basin are highly exaggerated. (bottom) Globally distributed oscillators within the ocean basin.

The water movement within the ocean basin means that the resultant water level change at a site on the ocean surface is determined by the water level changes at all sites on the surface. For example, the falling of a part of the basin instantly yields a water level change h_a for site A; simultaneously, the rising of another part of the basin instantly yields a water level change h_b

for site B. Under the effect of this pressure difference, water begins to move between these two sites, and the net, resultant water level change at site A would be expressed as $\Delta h=k_a h_a+k_b h_b$, where k_a and k_b are the contributing coefficients and determined by the influence of various factors, such as friction, reflection, the Earth's rotation, inertia, etc. When the ocean surface is divided into infinite sites, then the net, resultant water level change at any site *S* may be written as $\Delta h_s = \sum_{i=1}^{n} k_i h_i + k_s h_s$, where h_i is the water level change at the *i*th site on the surface due to the rising or falling of the basin's part beneath it, k_i is the contributing coefficient of the *i*th site, h_s is the water level change of site *S* that is due to the rising or falling of the basin's part beneath this site, and k_s is the contributing coefficient of site *S* itself. This relationship provides a theoretical basis to predict the tide.

To facilitate the following deduction, we consider a simple model in which the ocean basin is divided into a grid and the locations of these nodes of the grid act as oscillators (Figure 14(bottom)).We further assume that the water level change at every site of the ocean surface is instantly equal to the vertical displacement of the oscillator that is beneath it. Of course, the resulting water movement has feedback on solid Earth, for example, the water movement changes the weight distribution of the ocean, consequently, the elastic solid Earth reshapes itself as a response to this adjustment of weight. The response must be complicated, but its effect may be trivial with respect to the solid Earth deformation produced by the Moon's (Sun's) gravitational attraction, we here ignore this effect. Tide represents with a water level change around mean water level, and the influence of the water level change at a site on the water level change at another site cannot be instant due to the distance between the two sites, there would be time lag, the shallow water dynamics that may amplify tidal amplitude is also an important factor, and then, the tide height at any site *S* at time *t* may be approximately expressed as follows:

$$\Delta Y_{(t)} = Z_o + \sum_{i=1}^{n}\sum_{j=1}^{k} Qa_i b_j\,(lunar)\,\Delta Ha_i b_j\,(lunar)_{(t)} + \sum_{i=1}^{n}\sum_{j=1}^{k} Qa_i b_j\,(solar)\,\Delta Ha_i b_j\,(solar)_{(t)}$$
$$+Q_s\,(lunar)\,\Delta H_s\,(lunar)_{(t)} + Q_s\,(solar)\,\Delta H_s\,(solar)_{(t)} + D_s \qquad (2)$$

$$\Delta Ha_i b_j\,(lunar)_{(t)} = [(R+k_m)^2\, cos^2(\alpha_{a_i b_j} + \sigma_{a_i b_j}) + (R-k_m)^2\, sin^2(\alpha_{a_i b_j} + \sigma_{a_i b_j})]^{1/2} - R$$
$$\Delta Ha_i b_j\,(solar)_{(t)} = [(R+k_s)^2\, cos^2(\beta_{a_i b_j} + \mu_{a_i b_j}) + (R-k_s)^2\, sin^2(\beta_{a_i b_j} + \mu_{a_i b_j})]^{1/2} - R$$

$$\Delta Hs\left(lunar\right)_{(t)} = [\left(R + k_m\right)^2 cos^2\alpha_s + \left(R - k_m\right)^2 sin^2\alpha_s]^{1/2} - R$$

$$\Delta Hs\left(solar\right)_{(t)} = [\left(R + k_s\right)^2 cos^2\beta_s + \left(R - k_s\right)^2 sin^2\beta_s]^{1/2} - R$$

where Z_O is the average value of the tidal heights at site S over the period of the observations. D_s is the effect caused by the shallow water dynamics. $Qa_ib_j(lunar)$, $Qa_ib_j(solar)$, $Q_s(lunar)$, and $Q_s(solar)$ are the contributing coefficients of all related sites. n and k combine to represent the total number of the oscillators. $\Delta Ha_ib_j(lunar)_{(t)}$ and $\Delta Ha_ib_j(solar)_{(t)}$ are the water level changes at any other site a_ib_j in the lunar and solar deformations at time t, respectively; and $\Delta H_s(lunar)_{(t)}$ and $\Delta H_s(solar)_{(t)}$ are the water level changes at site S in the lunar and solar deformations, respectively; R is the mean radius of solid Earth, k_m and k_s are the lunar and solar deformations, respectively; $k_m=E_mQ_m(\cos\delta_m+\cos\Theta)$, $k_s=Q_s\cos\delta_s$, and $E_m=(R_{ME}/R_M)^2$, R_{ME} and R_M are the mean distance of the Moon from the Earth and the Moon's orbital radius, respectively; And δ_m, Θ, and δ_s are the Moon's declination, the angle between the Moon and Sun, and the Sun's declination, respectively. α_{aibj} and β_{aibj} are the lunar and solar angles of any other site a_ib_j, and α_s and β_s are the lunar and solar angles of site S; σ_{aibj} and μ_{aibj} are the phase lag of water level change influence between site S and any other site a_ib_j. $\cos\alpha=\sin\sigma\sin\delta_m+\cos\sigma\cos\delta_m\cos C_{mm}$ and $\cos\beta=\sin\sigma\sin\delta_s+\cos\sigma\cos\delta_s\cos C_{ms}$, where σ, δ_m, δ_s, C_{mm}, and C_{ms} are the geographic latitude of any site, the declination of the Moon, the declination of the Sun, the hour angle of any site with respect to the Moon, and the hour angle of any site with respect to the Sun, respectively. Equation (2) reflects a basic fact that, when the water level change of each of all the sites at the ocean surface is integrated, the sum of the water level changes of all the sites must be zero, this corresponds to a reality that the ocean as a whole is conservative in both mass and volume given water is incompressible and its density is constant. To simplify the calculation, especially in consideration of individual burden, we here select the locations of these nodes of a grid of 15°*15° to act as oscillators, with n=24 and k=11, and 187 oscillators are extracted. We adapt Q_m=0.19, Q_s=0.11, and the contribution of both shallow water dynamics and phase lag to water level change is ignored, namely, D_s=0, σ_{aibj} =0, μ_{aibj} =0. The grid is plotted with reference to both the equator and meridian, which allows the latitude and longitude of these oscillators to be easily known. Hourly tide-gauge data from 110 globally gauge sites (56 from GLOSS database - University of Hawaii Sea Level Center (UHSLC) (Caldwell et al., 2015), and 54 from National Oceanic and Atmospheric Administration (NOAA) of the U.S.A) are employed to test this

prediction model. The selected 54 NOAA stations are located mostly along the west and east coasts of U.S.A, while the selected 56 UHSLC stations cover most of oceans. More than hundreds of tide-gauge stations are presently listed in the online system of NOAA and are employing harmonic or subordinate method to do tide prediction, many of these stations are situated in the rivers and gulf coast, and the prediction data of some of these stations during September 2014 are not available. The selected 54 stations uniformly employ harmonic method, and their locations avoid the rivers and gulf coast. In particular, their prediction data during September 2014 are complete. These aspects lead our selection of these sample stations to be relatively reasonable. First, tide-gauge data covering a certain period of time and astronomical parameters are combined, by means of a least-squares fitting method, to resolve the contributing coefficients of Equation (2). Please note that we do not consider resolving Laplace's hydrodynamic equations in this study. Instead, we treat water movement as a black box, in which the boundary conditions are various factors, such as friction, reflection, the Earth's rotation, inertia, etc.; the input is the tide-gauge data; and the output is the contributing coefficients. Subsequently, we use the known contributing coefficients and Equation (2) to produce the tides during the following period of time. Hourly tide-gauge data 2014/08/01 to 2014/08/31 were used to resolve the contributing coefficients of Equation (2), and hourly tide-gauge data from 2014/09/01 to 2014/09/30 were used to compare the prediction in the month. To examine the strength of this model, we compare these predictions with those predictions that had been made by harmonic analysis in the past. The harmonic prediction for a location (i.e., port and island) is provided by the agency in the country that geographically holds this location. Many countries have now participated in IHO (International Hydrographic Organization), by an IHO agreement they exchange tide prediction data with each other. Among the selected 56 UHSLC tide-gauge stations, the prediction data of 10 stations can heretofore be found, these stations include Papeete, Rikitea, Nuku, Chichijima, Minamitorishia, Wllington, Bluff, Chatham, Qaqortoq, and Nuuk. But unfortunately, most of these stations have updated their tidal constituents, this leads the reproduced prediction data in the September 2014 to be unavailable. The available prediction data are finally kept for Chichijima and Minamitorishia that belong to Japan. Together with the prediction data of the selected 54 NOAA tide-gauge stations, 56 sample stations are finally used to do the prediction comparison between this model and harmonic analysis. The evaluation of the

results is realized in terms of the root mean square(*RMS*) of the amplitude. The *RMS* deviation for a tide-gauge site may be written as follows:

$$RMS = \sqrt{\frac{\sum_{i=1}^{m}\left(\Delta Y_{(t)-predicted} - \Delta Y_{(t)-observed}\right)^2}{m}} \tag{3}$$

where $\Delta Y_{(t)\text{-}predicted}$ and $\Delta Y_{(t)\text{-}observed}$ denote the in-phase amplitudes of the predicted and tide-gauge data, respectively, and m is the total number of tide-gauge data points during the period and equals 720.

The predicted tides out to observations and the prediction comparisons out to observations between this model and harmonic analysis are listed in Table 4, some of the predicted and observed tides are exhibited in Figure 15, and some of the prediction comparisons out to observations are exhibited in Figure 16. It can be found that the predicted tides are well consistent with the observed tides. The average *RMS* calculated against the observations for these 110 tide-gauge stations are 15.17 cm; The prediction made by this model is better than the prediction made by harmonic analysis. Among the selected 56 sample stations, the *RMS* calculated against the observations for 31 stations in this model is less than the *RMS* calculated in harmonic analysis.

Table 4(A) RMS calculated for 111 tide-gauge sites over different countries

	Tide-gauge station				RMS (cm)	
Item	ID Name	Latitude (°)	Longitude (°)	Country	Oscillation model	Harmonic analysis
Selected from GLOSS database	2 Betio (Tarawa)	1.35	172.92	Kiribati	8.25	not found
	3 Baltra	0.43	269.72	Ecuador	23.60	not found
	91 La	-2.20	279.08	Ecuador	13.93	not found
	5 Majuro	7.10	171.37	Marshall Islands	11.50	not found
	55 Kwajalein	8.73	167.73	Marshall Islands	9.40	not found
	7 Malakal	7.33	134.47	Belau	14.83	not found
	8 Yap	9.52	138.13	Fd. St. Micronesia	8.14	not found
	29 Kapingamarangi	1.10	154.78	Fd. St. Micronesia	15.76	not found
	15 Papeete	-17.53	210.43	French	7.48	unavailable
	16 Rikitea	-23.13	225.05	French	6.92	unavailable
	31 Nuku	-8.93	219.92	French	13.8	unavailable
	22 Easter	-27.15	250.55	Chile	16.38	unavailable
	80 Antofagasta	-23.65	289.6	Chile	10.38	unavailable
	81 Valparaiso	-33.03	288.37	Chile	15.86	unavailable
	83 Arica	-18.47	289.67	Chile	10.04	unavailable
	88 Caldera	-27.07	289.17	Chile	8.95	unavailable
	23 Rarotonga	-21.2	200.22	Cook Islands	7.93	not found
	24 Penrhyn	-8.98	201.95	Cook Islands	7.82	not found
	38 Nuku' alofa	-21.13	184.83	Tonga	12.99	not found
	46 Port Vila	-17.77	168.3	Vanuatu	9.75	not found
	47 Chichijima	27.1	142.18	Japan	11.43	41.38
	49 Minamitorishima	24.3	153.97	Japan	23.6	22.97
	71 Wellington	-41.28	174.78	New Zealand	20.65	unavailable
	72 Bluff	-46.6	168.33	New Zealand	27.86	unavailable
	79 Chatham	-43.95	183.43	New Zealand	20.41	unavailable
	93 Callao	-12.05	282.85	Peru	6.92	not found

	94 Matarani	-17.00	287.88	Peru	9.77	not found
	101 Mombasa	-4.07	39.65	Kenya	19.21	not found
	149 Lamu	-2.27	40.90	Kenya	30.38	not found
	103 Port Louis	-20.15	57.50	Mauritius	11.66	not found
	105 Rodrigues	-19.67	63.42	Mauritius	18.78	not found
	108 Hulhule	4.18	73.53	Republic of Maldives	5.83	not found
	109 Gan	0.68	73.15	Republic of Maldives	13.59	not found
	115 Colombo	6.97	79.87	Sri Lanka	6.74	not found
	119 Djibouti	11.60	43.15	Djibouti	15.90	not found
	121 Point La Rue	-4.67	55.53	Seychelles	9.17	not found
	122 Sibolga	1.75	98.77	Indonesia	10.28	not found

For latitudes, "-" denotes a site is located at the south of equator. "not found" denotes the prediction data during Sept 2014 cannot be found. "unavailable" denotes the prediction data have been found but are not available.

Table 4(B) (continue) RMS calculated for 110 tide-gauge sites over different countries

	Tide-gauge station				RMS (cm)	
Item	ID Name	Latitude (°)	Longitude (°)	Country	Oscillation model	Harmonic analysis
Selected from GLOSS database	125 Prigi	-8.28	111.73	Indonesia	13.51	not found
	124 Chittagong	22.23	91.83	Bangladesh	49.73	not found
	126 Jask	25.63	57.77	Iran	13.81	not found
	128 Thevenard	-32.15	133.63	Australia	22.65	not found
	142 Langkawi	6.43	99.75	Malaysia	21.77	not found
	147 Karachi	24.80	66.97	Pakistan	24.07	not found
	211 Ponta Delgada	37.73	334.32	Azores	10.37	not found
	223 Dakar	14.70	342.60	Senegal	20.41	not found
	235 Palmeira	16.70	337.00	Cape Verde	9.44	not found
	257 Settlement Point	26.72	281.00	United Kingdom	6.89	not found
	259 Bermuda	32.37	295.30	United Kingdom	11.68	not found

	276 St-John's	47.57	307.28	Canada	12.79	unavailable
	540 Prince Rupert	54.32	229.67	Canada	40.82	unavailable
	299 Qaqortoq	60.70	314.00	Greenland	30.67	unavailable
	329 Quarry Bay	22.30	114.22	Hong Kong, PRC	23.05	not found
	340 Kaohsiung	22.62	120.28	Taiwan	10.96	not found
	776 Punta Cana	18.50	291.62	Dominican Republic	4.81	not found
	803 Rorvik	64.87	11.25	Norway	30.98	not found
	820 Nuuk	64.17	308.28	Greenland/Denmark	27.15	unavailable
Selected from NOAA	1611400 Nawiliwili,	21.95	200.64	U.S.A	5.79	7.16
	1612340 Honolulu	21.31	202.13	U.S.A	5.29	11.5
	1619910 Sand Island	28.21	182.64	U.S.A	12.33	20.74
	1630000 Apra Harbor	19.29	166.62	U.S.A	6.25	6.39
	1770000 PAGO PAGO Harbor	-14.28	189.31	U.S.A	7.87	3.46
	1820000 KWAJALEIN ATOLL	8.73	167.74	U.S.A	9.49	8.35
	1890000 Wake Island	19.29	166.62	U.S.A	11.63	6.39
	8410140 Eastport, ME	44.90	293.02	U.S.A	48.35	11.48
	8411060 CUTLER FARRIS WHARF	44.66	292.80	U.S.A	30.08	10.56
	8413320 BAR HARBOR	44.39	291.80	U.S.A	27.66	9.45
	8418150 PORTLAND	43.66	289.76	U.S.A	24.69	9.53
	8423898 FORT POINT	43.07	289.29	U.S.A	22.98	10.77
	8461490 New London	41.36	287.91	U.S.A	9.83	9.53
	8510560 MONTAUK	41.05	288.04	U.S.A	9.54	11.62
	8518750 The Battery	40.70	285.99	U.S.A	13.62	14.21
	8531680 Sandy Hook	40.47	285.99	U.S.A	12.92	16.98
	8534720 Atlantic City	39.36	285.58	U.S.A	13.26	17.24

For latitudes, "-" denotes a site is located at the south of equator. "not found" denotes the prediction data during Sept 2014 cannot be found. "unavailable" denotes the prediction data have been found but are not available.

Table 4(C) (continue) RMS calculated for 111 tide-gauge sites over different countries

	Tide-gauge station				RMS (cm)	
Item	ID Name	Latitude (°)	Longitude (°)	Country	Oscillation model	Harmonic analysis
Selected from NOAA	8557380 Lewes	38.78	284.88	U.S.A	14.76	19.81
	8570283 Ocean City Inlet	38.33	284.91	U.S.A	12.19	17.34
	8632200 Kiptopeke Beach	37.17	284.01	U.S.A	15.07	18.90
	8651370 Duck	36.18	284.25	U.S.A	15.19	20.36
	8652587 OREGON INLET MARINA	35.80	284.45	U.S.A	8.87	17.34
	8656483 BEAUFORT, DUKE MARINE LAB	34.72	283.33	U.S.A	13.05	18.76
	8658163 Wrightsville Beach	34.21	282.21	U.S.A	17.11	20.86
	8670870 FORT PULASKI	32.04	279.10	U.S.A	22.45	20.81
	8720218 MAYPORT (BAR PILOTS DOCK)	30.40	278.57	U.S.A	18.10	16.13
	8721604 TRIDENT PIER, PORT CANAVERAL	28.42	279.41	U.S.A	14.30	15.15
	8722670 LAKE WORTH PIER	26.61	279.97	U.S.A	12.26	13.86
	8723214 Virginia Key	25.73	279.84	U.S.A	10.88	10.57
	8723970 VACA KEY, FLORIDA BAY	24.71	278.89	U.S.A	6.67	10.59
	8724580 KEY WEST	24.55	278.19	U.S.A	7.49	10.69
	9410170 SAN DIEGO (Broadway)	32.71	242.83	U.S.A	12.14	17.04
	9410230 La Jolla (Scripps Institution Wharf)	32.87	242.74	U.S.A	11.90	13.13
	9410660 LOS ANGELES (Outer Harbor)	33.72	241.73	U.S.A	11.28	13.27
	9410840 Santa Monica, Municipal Pier	34.01	241.50	U.S.A	10.99	13.46
	9411340 Santa Barbara	34.40	240.307	U.S.A	12.16	13.11

9412110 PORT SAN LUIS	35.17	239.246	U.S.A	12.04	9.96
9413450 MONTEREY, MONTEREY BAY	36.61	238.112	U.S.A	10.41	11.37
9114958 BOLINAS, BOLINAS LAGOON	37.91	237.3214	U.S.A	14.16	11.62
9414290 San Francisco	37.81	237.5341	U.S.A	11.59	11.39
9415020 Point Reyes	38.00	237.023	U.S.A	12.86	14.05
9416841 ARENA COVE	38.91	236.2889	U.S.A	12	15.05
9418767 HUMBOLDT BAY (North Spit)	40.77	235.783	U.S.A	18.98	23.22
9419750 CRESCENT CITY	41.75	235.82	U.S.A	15.28	10.16
9431647 PORT ORFORD	42.74	235.50	U.S.A	16.78	12.90
9432780 Charleston, OR	43.35	235.68	U.S.A	15.84	14.42
9441102 Westport	46.90	235.89	U.S.A	20.74	12.85
9442396 LA PUSH, QUILLAYUTE RIVER	47.91	235.36	U.S.A	20.96	14.23
9443090 NEAH BAY	48.37	235.40	U.S.A	18.70	11.24
94151600 SITKA	57.05	224.66	U.S.A	23.47	13.88
9457292 Kodiak Island	57.73	207.49	U.S.A	18.59	9.39
9461380 Adak Island	51.86	183.37	U.S.A	13.52	10.01
9755371 San Juan	18.46	293.88	U.S.A	6.94	9.88
9759938 MONA ISLAND	18.09	292.06	U.S.A	5.91	14.31

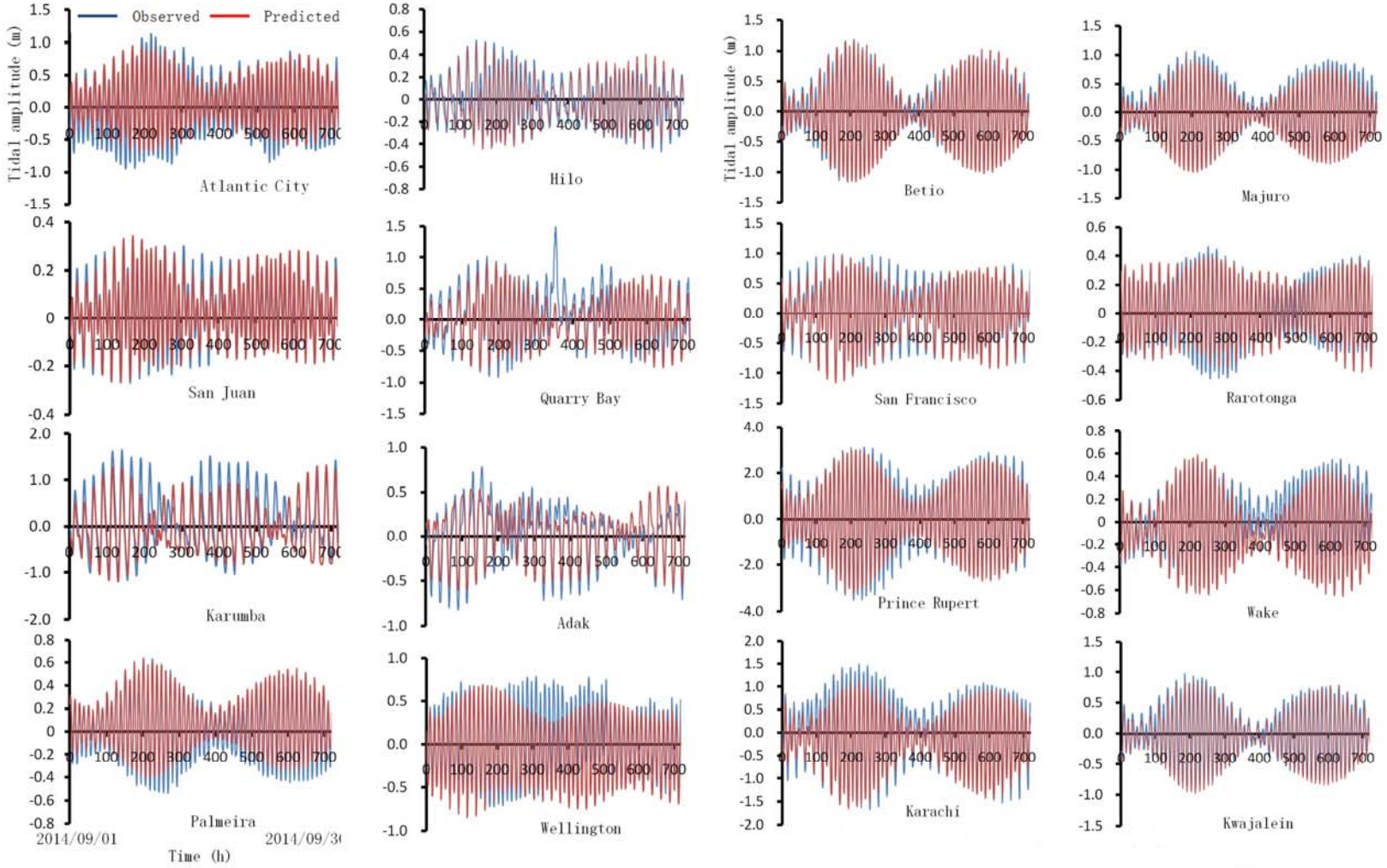

Figure 15. Representatives of the comparisons between the modeled and observed data from 2014/09/01 to 2014/09/30.

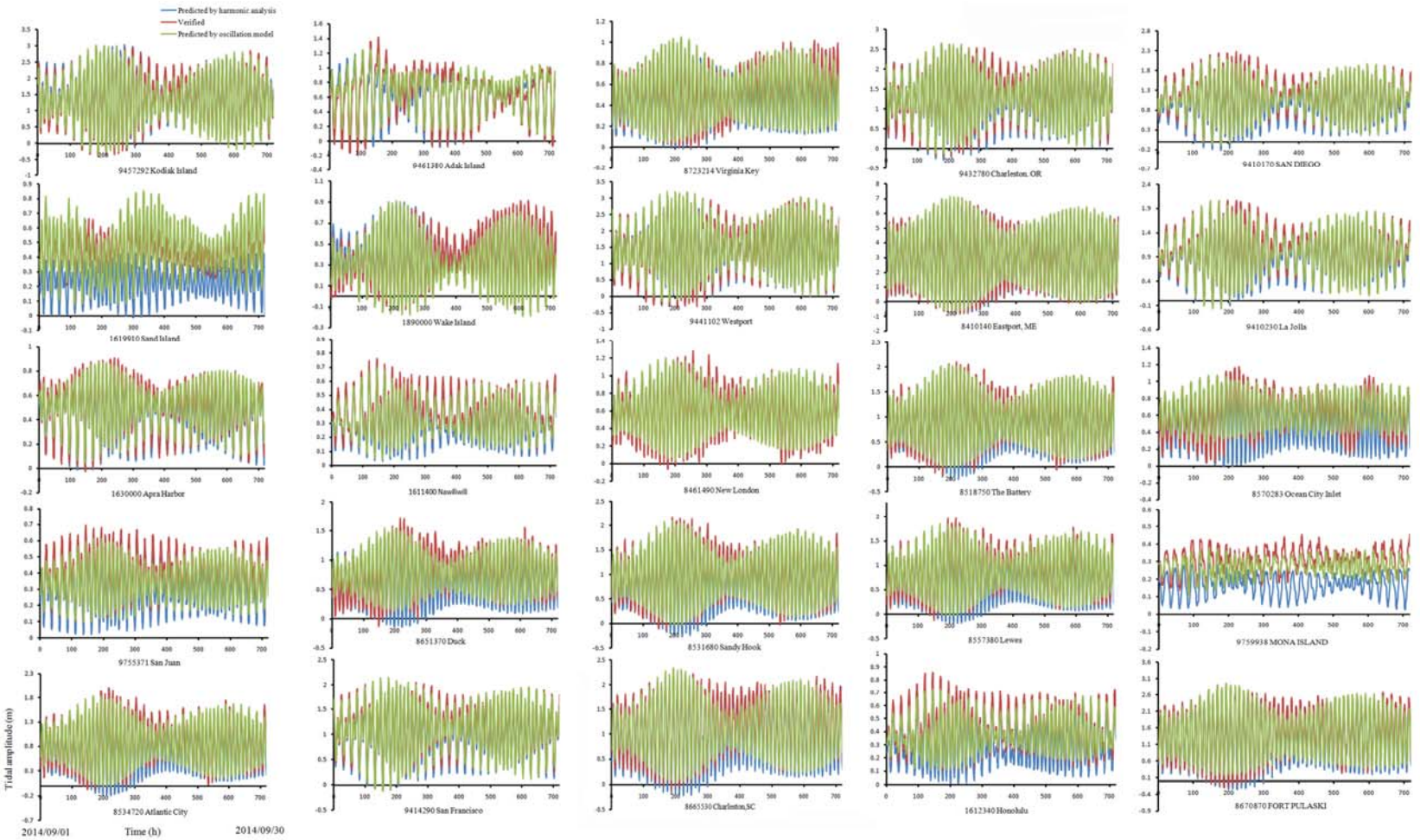

Figure 16. Comparison of the tides predicted by harmonic analysis and the tides predicted by oscillation model out to the observed/verified tides from 2014/09/01 to 2014/09/30.

4 Discussion

The misapplication of the tide-generating force to a watery Earth does not indicate that the gravitational attraction is wrong. Instead, as we are witnessing, the gravitational attraction performs well in guiding many activities such as land movement, satellite's orbit, and so on. The double solid bulge exhibited in the section 3.2 of this work is a good manifestation of the gravitational attraction. The absence of the double water bulge implies that the real impact of the Moon's (Sun's) gravitational attraction on the Earth's water cannot be identified. This work shows that even if we do not include this impact, the oceanic basin oscillation-driving mechanism can still independently explain the tides in both qualitative and quantitative manners. Some authors think that the gravitational model provides accurately tide predictions through harmonic analysis, this success in turn is the evidence that the gravitational model is correct. I asked myself many times whether the harmonic analysis is scientific/reasonable and may provide supporting for the gravitational model, the answer is not what they want, several points echo this light.

First of all, the tide prediction accuracy does not have a standard. The observed water levels at any location are always a combination of the astronomical tides plus non-tidal variances (e.g. wind, weather), these variances are irregular and usually not-repeating, tide predictions cannot include these irregular variances. Comparing tide predictions to observations leads to a wide variance in accuracy from a few centimeters to tens of centimeters. More detail about this matter may refer to an introduction of tide prediction accuracy in the website of NOAA (National Oceanic and Atmospheric Administration). Hence, the so-called accurately tide predictions themselves are plausible.

Second, we have used the tides predicted by harmonic analysis and the tides predicted by this oscillation model to compare with the observations, as shown in Figure 16 and table 4(B and C), the tide prediction made by oscillation model is entirely comparable to the tide prediction made by harmonic analysis. This reality leads to a point that a relatively accurate tide prediction is unnecessarily related to the gravitational model. One shouldn't neglect that a grid of $5^{o}*5^{o}$ in Figure 14 yields more than 1800 oscillators for the ocean basin, we only employ 187 oscillators to run the calculation. More oscillators still may be added to the calculation. In addition to this, the contribution of both the shallow water dynamics and the phase lag is not included in the

calculation. It is expectable that the inclusion of these aspects may realize a better accuracy for the oscillation model. Third, many people continue to regard the harmonic analysis and prediction as a black art, as did people in the earlier times. I fully agree this judgement. It is real that we have benefited from the tide prediction made through the harmonic analysis and should be grateful, but this method itself is mathematical other than physical. For a site, the harmonic analysis at first employs a trigonometric transform to decompose the potential equation into tens to hundreds of constituents (i.e., sinusoids), and each of these constituents is subsequently endowed two constants (i.e., amplitude and phase lag), by a least-square fitting to the observed tides, these constants are resolved. Casting the variance of time into these sinusoids of known constants, a simple addition of them obtains the water level change of this site at a future time. We see, this method is entirely a trick of math, it separates a site from the whole ocean and only makes use of a plus or subtract of number to obtain the water level change at the site. The continuity equation, as expressed with $\partial\zeta/dt+D(\partial u/\partial x+\partial v/\partial y)$, represents a basic fact that a net flux of water into or out of a site must be balanced by a corresponding change in the water level. An implication of this fact is that the water level change of a site is determined by the water level changes of all other sites within the whole ocean. In particular, the dynamic tide theory has concluded that the observed tides are a manifestation of the water movements. In the harmonic method, we cannot see where the inflow water comes from and where the outflow water goes to, what we can see is the water in the hands of a magician appears or disappears mysteriously. In contrast, the oscillation model treats the water level change of a site as a consequence of the water movements of all the sites within the ocean, it performs more scientific/reasonable than the harmonic method. To some extent, the oscillation model is the right choice for tide prediction in the future.

Last, attempting to use the harmonic analysis to support the gravitational model is not realistic. As demonstrated earlier, the tide-generating force is misapplied to a watery Earth, this leads the gravitational model to be groundless, the harmonic analysis is operated through the potential equation which is expressed with the gravitational model. As a result, such an endorsement is useless.

Newton described a tide (Proposition XXIV. Theorem XIX) in his book *Mathematical Principles of Natural Philosophy: "An example of all which Dr. Halley has given us, from the observations of seamen in the port of Batshom, in the Kindom of Tunquin (presently Viet Nam), in the latitude*

of 20°50' north. In that port, on the day which follows after the passage of the moon over the equator, the waters stagnate: when the moon declines to the north, they begin to flow and ebb, not twice, as in other ports, but once only every day: and the flood happens at the setting, and the greatest ebb at the rising of the moon. This tide increases with the declination of the moon till the 7th or 8th day; then for the 7 or 8 days following it decreases at the same rate as it had increased before, and ceases when the moon changes its declination, crossing over the equator to south. After which the flood is immediately changes into an ebb; and thenceforth the ebb happens at the setting and the flood at the rising of the moon; till the moon, again passing the equator, changes its declination. There are two inlets to this port and the neighboring channels, one from the seas of China, between the continent and the islands of Leuconia; the other from the Indian sea, between the continent and the island of Borneo. But whether there be really two tides propagated through the said channels, one from the Indian sea in the space of 12 hours, and once from the sea of China in the space of 6 hours, which therefore happening at the 3d and 9th lunar hours, by being compounded together, produce those motions; or whether there be any other circumstances in the state of those seas, I leave to be determined by observations on the neighbouring shores."

Newton attempted to provide an explanation for this tide, but his thought remains unverified. A similar phenomenon appears in Karumba of the Australian Gulf. The waters here flow and ebb dominantly once every day. When the Moon declines to the north, the greatest tide happens at the rising of the Moon; when the Moon changes its declination and crosses over the equator to the south, the greatest tide happens at the setting of the Moon. This kind of water movement is usually called the diurnal tide. Pugh and Woodworth (2014) depicted this kind of tide as a consequence of the Moon's declination, i.e., the declination produces an asymmetry between the two high and the two low water levels as a point rotates on the Earth within the two tidal bulges. This explanation cannot be realized in the frame of the two water bulges, because Karumba is located at the south of equator, when the Moon declines to the north, the two water bulges are always directed to the Earth-Moon line, the greatest tide should have happened at the setting of the Moon, and when the Moon changes its declination and crosses over the equator to the south, the greatest tide should have happened at the rising of the Moon. Of course, others explained the diurnal tide of Karumba with a scenario of the beating of O_1 and K_1 constituents (Pugh and Woodworth, 2014). Different from these existing understandings, we here demonstrate how the

diurnal tide may be a consequence of solid Earth deformation. As exhibited in Figure 17, when the Moon declines to the south, part of the southern ocean basin is raised by the first bulge at the rising of the Moon (Fig. 17(A)), which leads the water within this part to flow out. The water level at Karumba then falls, whereas some of the transferring water that moves towards north increases the water level in the port of Batshom. The raised part of the southern ocean basin begins to fall at the setting of the Moon, and at the same time, part of the northern ocean basin is raised by the second bulge (Fig. 17 (B)), which leads the water within it to flow out. Therefore, the water level in the port of Batshom falls while some of the transferring water that moves towards the south increases the water level at Karumba. When the Moon changes its declination and crosses over the equator to the north, the situation reverses. Because a pair of solid Earth bulges always tracks from east to west, part of the northern ocean basin is raised by first bulge at the rising of the Moon (Fig. 17(C)), which leads the water within this part to flow out. The water level in the port of Batshom then falls, and some of the transferring water that moves towards south increases the water level at Karumba. The raised part of the northern ocean basin begins to fall at the setting of the Moon, and at the same time, part of the southern ocean basin is raised by the second bulge (Fig. 17 (D)), which leads the water within this part to flow out. The water level at Karumba then falls, and some of the transferring water that moves towards the north increases the water level in the port of Batshom. When the Moon is over the equator, either the northern ocean basin or the southern ocean basin is slightly raised by these bulges. However, the water transferring between the northern ocean basin and the southern ocean basin is tiny; thus, the waters in the port of Batshom and at Karumba may be stagnated.

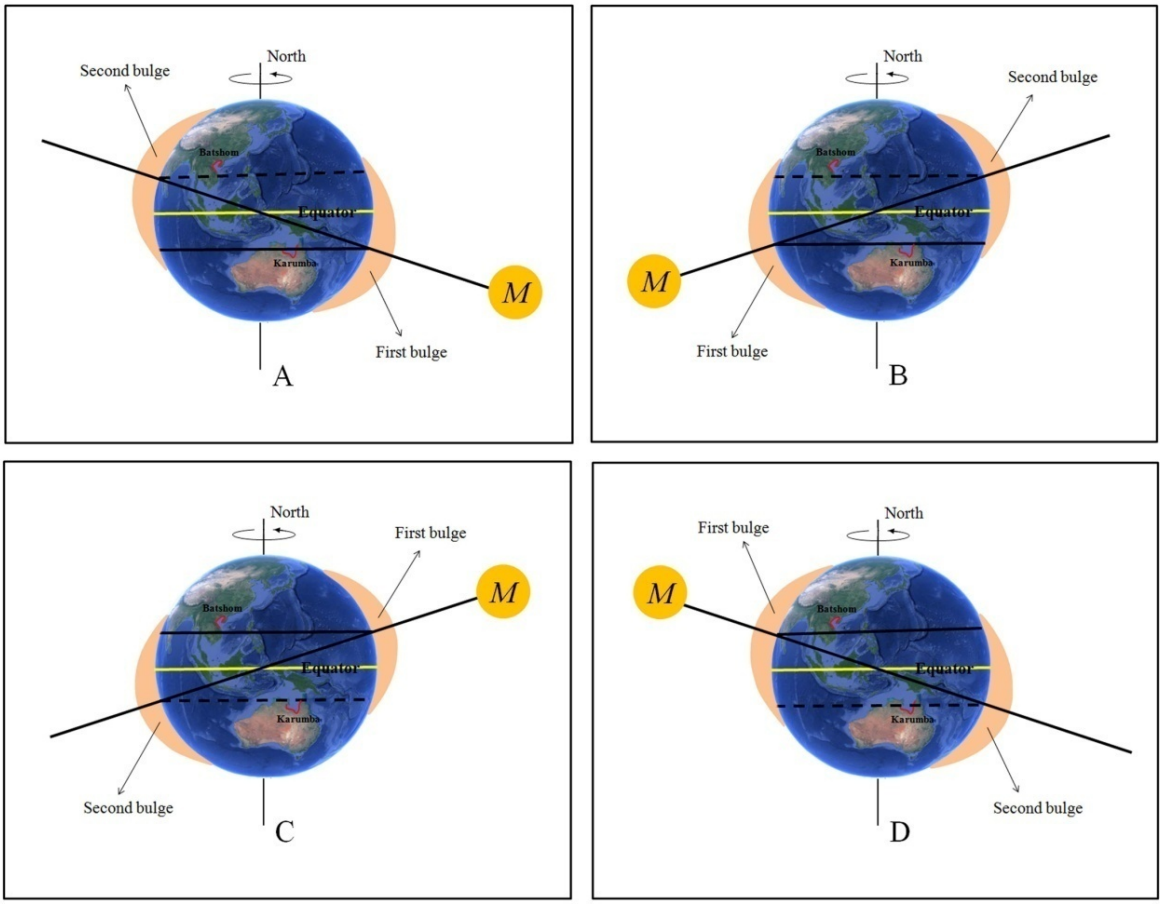

Figure 17. Modeling the formation of diurnal tide at Batshom and Karumba because of the oceanic basin oscillation.

The study of Solid Earth deformation has a long history and may track back to two centuries ago, many people including Lord Kelvin and George Darwin had made great contribution to this issue. Love in detail presented the yielding of solid Earth to the external forcing and related Earth tide to the rigidity that is determined by the matter within the Earth (Love, 1909). After that, Longman introduced a Green's function to calculate the load tide that is a part of the Earth tide (Longman, 1963); Several authors revaluated the responses of solid Earth to tide-generating forces and ocean tide (Farrell, 1973; Hendershott, 1972; Melchior, 1974; Agnew, 1981; Scherneck, 1991). The main conclusions obtained include: the deformation of solid Earth by ocean tide results in load tides in tilt, strain, and vertical acceleration; Tidal forces yield stress for the Earth, and the stress-strain relation for rock is nonlinear; The weight of the oceanic tidal

column can have influence on the deformation of solid Earth. The current view is that the contribution of Earth tide to ocean tide can be expressed by (1+k-h)Ωp/g, where Ωp/g is the equilibrium tide amplitude and (1+k-h) is a combined diminishing factor in the equilibrium tide (Pugh, 1987; Pugh and Woodworth, 2014). This expression indicates that Earth tide and the equilibrium tide are similar in shape, and the contribution of Earth tide to ocean tide is a simple addition of tide amplitude. Different from these established understandings, in this work we demonstrate the Earth tide itself may independently explain ocean tide.

Acknowledgments

We are very grateful to Philip Woodworth and John Huthnance for their helpful comments on this work. We thank Walter Babin, Thierry De Mees, Roger A. Rydin, and Wouter Schellart for their suggestions on earlier versions of the text. We thank JiaJia Yuan for helping obtain altimetry data from AVISO and providing map of satellite ground tracks, and for his comments on this work. It is grateful to Richard Ray for providing the image of M_2 tide. We also thank Hartmut Wziontek and Calvo Marta for their valuable discussions on gravity data. Todd Ehret of U.S. NOAA is highly appreciated for the aid and discussion of tide prediction. Michael G. Hart-Davis, Carolina Calvete, Glen Rowe, Mads Hvid Ribergaard, Claire Fraboul, and Miwako Yoritaka are appreciated for providing tide prediction data. We also thank the following institutions for their data support: U.S. NOAA, NASA's JPL, GLOSS database - University of Hawaii Sea Level Center (UHSLC), and GGP (Global Geodynamics Project).

Data Availability Statement

The tide-gauge data used for testing the double water bulge in this study are available through Caldwell et al., 2015. The satellite altimetry data used for testing the double water bulge are available at AVISO (ftp://ftp-access.aviso.altimetry.fr). The gravity data used for testing the double solid bulge are available through Voigt et al., 2016, and the bottom pressure data used for testing the double solid bulge are available at NDBC, NOAA (https://www.ndbc.noaa.gov). The tide-gauge data used for comparing the tide prediction are available through Caldwell et al., 2015, Oceanographic Data Exchange of Japan (https://www.data.jma.go.jp/gmd/kaiyou/db/tide/suisan/), and at NOAA (https://tidesandcurrents.noaa.gov/stations.html?type=Datums).

References

Agnew, D. C. (1981). Nonlinearity in rock - Evidence from Earth tides. *J. geophys. Res*., 86, 3969-3978.

Caldwell, P. C., Merrifield, M. A., Thompson, P. R. (2015). Sea level measured by tide gauges from global oceans - the Joint Archive for Sea Level holdings (NCEI Accession 0019568), Version 5.5, *NOAA National Centers for Environmental Information*, Dataset, doi:10.7289/V5V40S7W.

Cartwright, D. E. (1999). Tides: A Scientific History. Cambridge University Press, Cambridge.

Deacon, M. (1971). Scientists and the Sea, 1650-1900. Academic Press (London).

Doodson, A. T., and Warburg, H. D. (1941). Admiralty Manual of Tides, London HMSO.

Farrell, W. E. (1973). Earth tides, ocean tides and tidal loading. *Philosophical Transactions of the Royal Society of London*, A274, 253-259.

Fowler, C. M. R. (2004). The Solid Earth: An Introduction to Global Geophysics (2nd Education). Cambridge University Press, Cambridge.

Fok, H. S. (2012). Ocean Tides Modeling using Satellite Altimetry. Ohio State University.

Fu, L.-L., and Cazenave, A. (2001). Satellite Altimetry and Earth Sciences. Academic Press, San Diego, Calif.

Gao, Z. Z., He, Y. B., Li, X. D., and Duan, T. Z. (2013). Review of research in internal-wave and internal-tide deposits of China. *Journal of Palaeogeography*, 2 (1), 56-65.

Gargett, A. E., Hughes, B. A. (1972). On the interaction of surface and internal waves. *Journal of Fluid Mechanics*, 52, 179-191.

Garrett, C., Munk,W. (1979). Internal waves in the ocean. *Annual Review of Fluid Mechanics*, 1, 339-369.

Gerkema, T. (2019). An introduction to tides. Cambridge University Press.

Hart-Davis, M. G., Piccioni, G., Dettmering, D., Schwatke, C., Passaro, M., Seitz, F. (2021). EOT20: a globl ocean tide model from multi-mission satellite altimetry. *Earth Syst. Sci. Data*, 13, 3869-3884.

Hendershott, M. C. (1972). The effects of solid Earth deformation on global ocean tides. *Geophysical Journal of the Royal astronomical Society*, 29, 389-402.

Kaula, W. M. (1968). Introduction to Planetary Physics: the Terrestrial Planets. John Wiley.

Kopal, Z. (1969). Dynamics of the Earth-Moon System. Springer Netherlands.

Lide, D. R. (2000). Handbook of Chemistry and Physics (81st ed.).

Longman, I. M.(1963). A Green's function for determining the deformation of the Earth under surface mass loads. *J. geophys. Res.*, 68, 485-496.

Love, A. E. H. (1909). The Yielding of the Earth to Disturbing Forces. *Proc. Roy. Soc. London*, 82, 73-88.

Luzum, B., Capitaine, N., Fienga, A., Folkner, W., Fukushima, T., Hilton, J., Hohenkerk, C., Krasinsky, G., Petit, G., Pitjeva, E., Soffel, M., Wallace, P. (2011). The IAU 2009 system of astronomical constants: The report of the IAU working group on numerical standards for Fundamental Astronomy. *Celestial Mechanics and Dynamical Astronomy*, 110(4), 293-304.

Melchior, P. (1974). Earth Tides. *Surveys in Geophysics*, 1, 275-303.

National Research Council (U.S.). (1993). Solid-Earth sciences and society. National Academy Press, Washington.

Pekeris, C. L., and Accad, Y. (1969). Solution of Laplace's equations for the M_2 tide in the world oceans. *Philos. Trans. R. Soc. A.*, *A265*, 413-436.

Phillips, O. M. (1974). Nonlinear dispersive waves. *Annual Review of Fluid Mechanics*, 6, 93-110.

Pidwirny, M.(2006). Introduction to the Oceans (Fundamentals of Physical Geography, 2nd Edition).

Pugh, D. T. (1987). Tides, Surges and Mean Sea-Level. JOHN WILEY & SONS.

Pugh, D. T. and Woodworth, P. L. (2014). Sea-Level Science: Understanding Tides, Surges Tsunamis and Mean Sea-Level Changes. Cambridge Univ. Press, Cambridge.

Robert, H. S. (2008). Introduction To Physical Oceanography. Texas A& M University.

Roy, A. E. (1978). Orbital Motion. Adam Hilger, Bristol.

Scherneck, H. -G. (1991). A parametrized solid Earth tide model and ocean tide loading effects for global geodetic baseline measurements. *Geophys. J. Int.*, 106(3), 677-694.

Schureman, P. (1940). Manual of Harmonic Analysis and Prediction of Tides. Washington, U. S. Coast and Geodetic Survey, Spec. Publ. No. 98.

Schureman, P. (1976). Manual of Harmonic Analysis and Prediction of Tides. United States Government Printing Office, Washington.

Schwiderski, E. W. (1979). Global ocean tides: Part II. The semidiurnal principal lunar tide 84 (M_2), Atlas of Tidal Charts and Maps, NSWC Tech. Rep., 79-414.

Shanmugam, G. (2014). Review of research in internal-wave and internal-tide deposits of China: Discussion. *Journal of Palaeogeography*, 3, 332-350.

Shepard, F. P. (1975). Progress of internal waves along submarine canyons. *Marine Geology*, 19, 131-138.

Shum, C. K.,Woodworth, P. L., Andersen, O. B., Egbert, G. D., Francis, O., King, C., Klosko, S. M., Le Provost, C., Li, X., Molines, J. -M., Parke, M. E., Ray, R. D., Schlax, M. G., Stammer, D., Tierney, C. C., Vincent, P., Wunsch, C. I. (1997). Accuracy assessment of recent ocean tide models. *J. Geophys. Res.*, 102, 25,173-25,194.

Simon, J. L., Bretagnon, P., Chapront, J., Chapront-Touze, M., Francou, G., Laskar, J. (1994). Numerical expressions for precession formulae and mean elements for the Moon and planets. *Astronomy and Astrophysics*, 282 (2), 663-683.

Smart, W. M. (1940). Spherical Astronomy. Cambridge University Press.

Stammer, D., Ray, R. D., Andersen, O. B., Arbic, B. K., Bosch, W., Carrère, L., Cheng, Y., Chinn, D. S., Dushaw, B. D., Egbert, G. D., Erofeeva, S. Y., Fok, H. S., Green, J. A. M., Griffiths, S., King, M. A., Lapin, V., Lemoine, F. G., Luthcke, S. B., Lyard, F., Morison, J., Müller, M., Padman, L., Richman, J. G., Shriver, J. F., Shum, C. K., Taguchi, E., Yi, Y. (2014). Accuracy assessment of global barotropic ocean tide models. Rev. Geophys., 52, 243-282.

Visser, P. N. A. M., Sneeuw, N., Reubelt, T., Losch, M., Van Dam, T. (2010), Space-borne gravimetric satellite constellation and ocean tides: Aliasing effects. *Geophys. J. Int.*, 181, 789-805.

Voigt, C., and Coauthors.: Report on the Data Base of the International Geodynamics and Earth Tide Service (IGETS),
(Scientific Technical Report STR – Data; 16/08), Potsdam: GFZ German Research Centre for Geosciences.DOI:doi.org/10.2312/GFZ.b103-16087, 2016.

Wieczorek, M. A., and Coauthors.: The constitution and structure of the lunar interior, Reviews in Mineralogy and Geochemistry, 60(1), 221-364, 2006.

Williams, D. R.: Sun Fact Sheet, NASA Goddard Space Flight Center, 2013.